ST. ANTHONY FALLS HYDRAULIC LABORATORY
UNIVERSITY OF MINNESOTA

Project Report No. 48

THE DISTRIBUTION OF AIR IN SELF-AERATED FLOW IN A SMOOTH OPEN CHANNEL

Submitted by
LORENZ G. STRAUB
Director

Prepared by
ALVIN G. ANDERSON

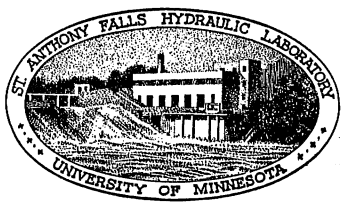

July 1955

Prepared for
OFFICE OF NAVAL RESEARCH
Department of the Navy
Washington, D.C.

Office of Naval Research Contract N6onr-246 Task Order VI

P R E F A C E

Contract N6onr-246, Task Order VI, between the Office of Naval Research and the University of Minnesota specified that the St. Anthony Falls Hydraulic Laboratory "conduct research on the basic mechanisms whereby atmospheric air is entrained into water by the relative motion of the two fluids." This report is one of a series in fulfillment of this order. Previous reports pertaining to this program have summarized the literature related to the subject, and have described the special apparatus and instruments developed and fabricated in the course of this investigation to measure the air content and the high velocities inherent in the phenomenon. The present report presents the results and analysis of experiments to measure the air concentration distribution in a smooth channel for a variety of flow conditions.

The air entrainment investigation is under the general direction of Dr. Lorenz G. Straub, director of St. Anthony Falls Hydraulic Laboratory. The present study, as a part of a continuing program, was under the supervision of and the report prepared by Alvin G. Anderson. Important assistance in the collection and analysis of data was rendered by Alan S. Goodyear and Jimmie F. Hayek, research assistants. Howard Jongedyk, Courtland Mueller, and Donald Kjellman worked on the project for shorter periods. Professor E. Silberman critically reviewed the draft of the report.

A B S T R A C T

The high-velocity self-aerated flow in an open channel is characterized by the appearance of "white water" caused by the entrainment of atmospheric air. The phenomenon appears to be made up of two parts. In the lower portion of the flow the entrained air is in the form of bubbles distributed through the flow. Above this region, water particles projected outward from the flow by the intense normal velocity fluctuations give rise to the highly agitated appearance of the flow.

Properties and parameters of the distribution curve are correlated with the bulk flow characteristics. The mean depth for the smooth channel based upon the air distribution appears to be a function of the ratio of unit water discharge and the square root of the slope, $q/S^{1/2}$. It was found empirically that the mean air concentration is related to the parameter $S/q^{2/3}$ which is related to $V_*/(\bar{d})^{5/4}$ and which implies that it increases with the shear velocity and decreases with the mean depth. The proportion of the total water flow occurring in the region below the mean depth is also related to $S/q^{2/3}$ approaching 1.0 for small values and decreasing to 0.6 for the largest measured value of $S/q^{2/3}$. The results indicate that the resistance to aerated flow is less than unaerated flow. Based upon the mean depth, these results indicate that the resistance to aerated flow is about 70 per cent of that for unaerated flow.

An approximate analysis of the air-concentration distribution based upon the turbulence of the flow has been made for the upper region and for the lower regions separately.

CONTENTS

	Page
Preface	iii
Abstract	iv
List of Illustrations	vi
List of Symbols	viii
I. INTRODUCTION	1
II. DESCRIPTION OF EXPERIMENTS	2
A. Apparatus	2
B. Experimental Procedure	4
III. EXPERIMENTAL RESULTS	4
A. Distribution Curves	4
B. Depth of Flow	11
C. Air Concentration	12
IV. ANALYSIS OF EXPERIMENTAL DATA	16
A. Relation Between Depth of Flow, Discharge, and Slope	16
V. SUMMARY AND CONCLUSIONS	20
Bibliography	23
Appendix A - Analysis of Air-Concentration Distribution	33
Appendix B - Graphical Presentation of Experimental Measurements	45

LIST OF ILLUSTRATIONS

Figure		Page
1	General View of Channel for Air-Entrainment Experiments	25
2	Air-Concentration Meter Used in High-Velocity Flow	25
3	Example of Differences in Air-Concentration Profiles	26
4	Typical Experimental Concentration Distribution	26
5	Mean Depth as a Function of Discharge	27
6	Maximum Depth as a Function of Discharge	27
7	Depth of 50 Per Cent Air Concentration as a Function of Discharge	28
8	Mean Air Concentration of Total Flow as a Function of Discharge	28
9	Mean Depth as a Function of $q/S^{1/2}$	29
10	Depth of 50 Per Cent Air Concentration as a Function of $q/S^{1/2}$	29
11	Depth of Unaerated Flow as a Function of $q/S^{1/2}$	29
12	Friction Factor as a Function of Reynolds Number for Unaerated Flow	30
13	Friction Factor as a Function of Reynolds Number	30
14	Maximum Depth as a Function of $\bar{V}/S^{1/2}$	30
15	Mean Concentration of Total Flow as a Function of $S/q^{2/3}$ . . .	31
16	Mean Concentration of Total Flow as a Function of $V_*/(\bar{d})^{5/4}$	31
17	Relative Discharge Below Mean Depth as a Function of $S/q^{2/3}$	31
A-1	Measured Air Concentration Plotted as a Probability Function	41
A-2	Variation of h/d_{50} as a Function of $S/q^{2/3}$	41
A-3	Measured Air Concentration in Lower Region of Flow	41
A-4	Constant C_o (Eq. A-11) as a Function of Parameter $S/q^{2/3}$ . .	42
A-5	Exponent z (Eq. A-11) as a Function of Parameter $S/q^{2/3}$ . . .	42
B-1	Air-Concentration Distribution Slope 7.5°	48
B-2	Air-Concentration Distribution Slope 15°	50
B-3	Air-Concentration Distribution Slope 22.5°	52
B-4	Air-Concentration Distribution Slope 30°	54

Figure Page

B-5 Air-Concentration Distribution Slope 37.5°. 56

B-6 Air-Concentration Distribution Slope 45°. 58

LIST OF SYMBOLS

C - Concentration, ratio of volume of air to volume of air plus water.

$\bar{C}$ - Mean concentration in vertical section.

C_o - Concentration at point $y = d_T/2$.

$\bar{C}_1$ - Mean air concentration in region between lower boundary and $\bar{d}$.

C_T - Concentration at transition depth $y = d_T$.

$\bar{d}$ - A mean depth of flow if all entrained air were removed.

$d_{0.50}$ - Distance from channel bottom or value of y where $C = 0.5$.

d_u - Distance from channel bottom or value of y where $C = 0.99$.

d_T - Transition depth between upper and lower regions of flow.

d_e - Depth at inlet to flume.

d_m - Mean depth in unaerated flow.

d_a - An effective depth of aerated flow such that resistance coefficient is same as for unaerated flow.

f - Darcy friction coefficient.

g - Acceleration due to gravity.

h - A mean height to which water particles are projected above d_T.

k - Kármán universal constant for velocity distribution.

$N_{y'}$ - Number of particles reaching or passing through a horizontal area a distance y' above transition depth d_T.

N_T - Number of particles that leave or return to an area at the transition depth.

$P_{y'}$ - Proportion of all particles leaving area at transition depth that reach or pass through horizontal area at y' above transition depth.

Q - Total water discharge.

q - Water discharge per unit width of channel.

q_1 - Water discharge per unit width flowing between lower boundary and $\bar{d}$.

R - Hydraulic radius.

Re - Reynolds number.

S - Slope of channel bottom, $S = \sin \alpha$.

V - Local velocity.

$\bar{V}$ - Mean velocity in vertical section = $q/(\bar{d})$.

V_* - Shear velocity = $\sqrt{g(\bar{d})} \sin \alpha$.

V_b - Rising velocity of air bubbles.

y - Normal distance from channel bottom.

y' - Normal distance from transition depth.

z - Exponent in air concentration equation.

α - Angle of inclination of channel.

β - Constant.

ϵ_b - Mixing coefficient for air bubbles in turbulent flow.

ϵ_m - Mixing coefficient for momentum transfer.

ν - Kinematic viscosity of water.

ρ - Density of water.

τ - Local shear force.

τ_o - Boundary shear force.

THE DISTRIBUTION OF AIR IN SELF-AERATED FLOW IN A SMOOTH OPEN CHANNEL

I. INTRODUCTION

This report is one of a series resulting from an investigation of the mechanics by which air is entrained in high-velocity open-channel flow. Previous reports pertaining to this program at the St. Anthony Falls Hydraulic Laboratory of the University of Minnesota have summarized the literature published on the subject [1]*, and have described the special apparatus [2] and instruments [3] [4] developed and fabricated in the course of this investigation to measure the air content and the high velocities inherent in the phenomenon.

The entrainment of air into open-channel flows of high velocity is characterized by the appearance of "white water" and the violent agitation of the flow. The upper surface, as such, becomes indeterminate and the air content varies, not only with the flow conditions such as discharge, slope, and roughness, but also within the flow itself with respect to distance from the fixed bed. These characteristics have been well described in a previous paper [5] based upon preliminary measurements of air concentration and velocity distribution, and from observations by other authorities. It has been reasonably well established that for flows over a spillway from a low turbulence reservoir, incipient aeration does not occur until a point is reached where the boundary layer intersects the stream surface. The characteristic roughening of the water surface immediately upstream of the appearance of "white water" can be readily observed in such installations. With increasing initial depths, the point where the roughening and the "white water" occur moves downstream. This suggests that aeration is related to the conditions of turbulence in the flow. Examinations of the surface in high-speed photographs indicate that at any instant the surface is made up of depressions and spikes of aerated water in apparently random order. In the process of creating this rough surface, air is entrapped and carried into the flow. It is then distributed through the flow by the process of turbulent mixing created by the velocity

*Numbers in brackets refer to the Bibliography on p. 23.

fluctuations. The turbulent mixing is counteracted by the buoyancy of the air bubbles so that an equilibrium is reached in the entrapment and liberation of air. Above the zone of turbulent mixing, the masses of water or aerated water are projected into the atmosphere; and since there is no mechanism for maintaining them in the atmosphere, they will fall back into the flow at the end of their trajectory downstream. Preliminary measurements of air concentration show that the air concentration increased continuously from the bed, exhibiting smooth transitions from the concentration near the bed, to 100 per cent air concentration which is approached asymptotically. Earlier investigators have pictured air-entrained flow as being made up of air bubbles entrained in water at the lower levels, and water particles in the air in the upper regions.

This report presents the results of measurements of the air content and its distribution in a centerline section at the end of the experimental channel for a number of water discharges and slopes.

II. DESCRIPTION OF EXPERIMENTS

A. Apparatus

The experiments were carried out in a channel [2] 50-ft long, 1.5-ft wide, and 1-ft deep, which could be adjusted at any slope from horizontal to nearly vertical. The width was chosen so that sidewall effects due to growth of the sidewall boundary layer and air entrainment along the sides could be avoided in the central portion of the cross section. That the width was adequate to make the flow two-dimensional in the center portion was demonstrated by earlier measurements of air concentration and velocity in a transverse section at the end of the flume [5]. The discharge was obtained from the Laboratory supply flumes through two feed lines and controlled by hydraulically operated valves. The water reached the inlet of the flume through hollow support members and through a rectangular conduit on the underside of the channel. Figure 1 shows the apparatus.

At the inlet, the flow is guided through two, 90-degree vaned bends and a contraction to the inlet gate. The inlet gate itself is cantilevered from its mounting at the top of the flume so that there are no slots or guides to disturb the flow. Further guidance is provided by a lip attached to the

bottom of the gate and extending inward to further contract the flow; therefore, the gate opening corresponds to the depth of flow at the exit. The maximum gate opening is 6 inches. Pitot measurements of the flow just downstream of the inlet with a 3-in. gate opening showed no deviation greater than 2 per cent from the mean velocity, except in the bottom corners, where slightly smaller velocities were encountered.

The discharge itself was measured by two, calibrated Pitot cylinders mounted in the supply lines and leading to differential gages mounted on the control panel. Each discharge meter was calibrated separately for flows from 1/2 to 10 cfs with an accuracy in the neighborhood of 1 per cent.

A control panel contained the actuating components for the hydraulic system, and indicators for the measurement of slope, gate opening, and discharge, which permitted adjustment of these variables to predetermined values.

The electrical air-concentration measuring instrument has been fully described in an earlier report [3]. The method consists basically of a measurement of the difference between the conductivity of a mixture of air and water, and the conductivity of water alone. A strut supporting a pair of probes is combined with the electrical circuit so that the air concentration measurements may be made in a small region of the flow. The probes are 1/4-in. wide and 1/4 in. apart. The instrument is direct reading, and the relation between conductivity and air concentration can be determined analytically. The strut holding the probes is arranged so that it is possible to traverse the flow cross section both vertically and laterally. The instrument is limited to measurements not closer than 0.02 ft from the walls because of current deflections by the walls at lesser distances. Since the measurements of the air concentration depend upon the resistance or specific sensitivity of the suspending fluid, the meter was zeroed in unaerated fluid continually circulated from the channel flow through a tank, thus providing water of the same character as that in the flume. Oscilloscope measurements show a rapidly fluctuating current between the probes. Since the meter could not follow these rapid fluctuations, the value read on the meter represented an average value. This average compared well with results obtained by means of a mechanical sampler which was not subject to the same averaging problems. A photograph of the probes and strut supports for the air-concentration meter is presented in Fig. 2.

B. Experimental Procedure

For the air distribution measurements described in this report, the slope and water discharge were varied independently. Experiments were made for slopes of 7.5, 15, 22.5, 30, 37.5, and 45 degrees. For each slope, measurements of air concentration were made for total water discharge of 3.2, 4.2, 5.2, 6.4, 7.2, 8.2, and 9.6 cfs. All of the reported measurements were made for a single channel roughness, that of the painted-steel plates of the channel bottom and sides.

The measurements were made at station 45 (45 ft from the inlet) in a vertical centerline plane. Readings were taken at 1/8-in. intervals on a line normal to the bottom, starting at a point 1/4 in. from the bed, and continuing until the probes were completely out of the flow, and the meter registered zero water concentration. The profile was obtained for each slope and each water discharge after the channel had been adjusted for equilibrium conditions. For this purpose, equilibrium flow was considered to be that condition of the flow of the air-water mixture for which the air-concentration distribution was the same at two sections 10 ft apart. For this channel, this condition could be obtained by the adjustment of the initial depth of flow through control of the inlet gate opening. Repeated measurements of the profiles were made at the two sections for different gate openings until the two profiles were similar. The entrance depth, d_e, for equilibrium is listed in Table II, Column 7. Comparisons were made of the concentration at corresponding distances normal to the bed. A comparison of the profiles at the two stations for equilibrium flow is shown in Fig. 3.

III. EXPERIMENTAL RESULTS

A. Distribution Curves

The results of the air-concentration measurements taken at station 45 on the channel centerline in the two-dimensional region for equilibrium flow are tabulated in Table I for each discharge and each slope. A typical curve showing air concentration as a function of depth is presented in Fig. 4. Similar curves for all of the runs tabulated in Table I are shown in Figs. B-1 to B-7 of Appendix B. The concentration of air, C, is defined as the ratio of the volume of air per unit volume of air and water, as measured by the

TABLE I

CONCENTRATION OF AIR AT VARIOUS DISTANCES FROM THE BED

Run Nos. 161-167
Slope 7.5°

Distance from Channel Bed (ft)	Run - 161	162	163	164	165	166	167
	T* = 0.2	0.2	0.2	0.2	1.0	1.3	0.3
	Q** = 3.2	4.2	5.2	6.4	7.2	8.2	9.6
0.021	0.04	0.03	0.03	0.04	0.03	0.04	0.03
0.031	0.02	0.03	0.02	0.03	0.02	0.02	0.02
0.042	0.02	0.02	0.02	0.03	0.02	0.02	0.02
0.052	0.02	0.02	0.02	0.03	0.01	0.02	0.02
0.063	0.02	0.02	0.02	0.03	0.01	0.02	0.02
0.073	0.03	0.03	0.02	0.03	0.01	0.02	0.02
0.083	0.05	0.03	0.02	0.03	0.01	0.02	0.02
0.094	0.12	0.05	0.02	0.03	0.02	0.02	0.02
0.104	0.23	0.07	0.03	0.03	0.02	0.02	0.02
0.115	0.41	0.14	0.05	0.04	0.02	0.02	0.02
0.125	0.62	0.25	0.10	0.05	0.03	0.03	0.02
0.135	0.82	0.41	0.18	0.06	0.04	0.04	0.02
0.146	0.92	0.61	0.30	0.13	0.05	0.05	0.03
0.156	0.97	0.74	0.48	0.22	0.11	0.06	0.04
0.167	0.99	0.84	0.67	0.38	0.20	0.07	0.05
0.177		0.93	0.78	0.52	0.34	0.12	0.06
0.188		0.97	0.88	0.65	0.48	0.17	0.09
0.198		0.98	0.94	0.78	0.58	0.32	0.16
0.208			0.97	0.85	0.74	0.45	0.25
0.219			0.98	0.92	0.85	0.60	0.35
0.229			0.99	0.96	0.90	0.73	0.51
0.240				0.98	0.95	0.82	0.60
0.250				0.99	0.97	0.90	0.71
0.260					0.98	0.94	0.82
0.271						0.96	0.88
0.281						0.98	0.93
0.291						0.99	0.95
0.302							0.98
0.312							0.99

*Temperature in degrees Centigrade.

**Discharge in cfs.

TABLE I (Cont.)

CONCENTRATION OF AIR AT VARIOUS DISTANCES FROM THE BED

Run Nos. 141-147
Slope 15°

Distance from Channel Bed (ft)	Run - 141	142	143	144	145	146	147
	T* = 5.5	7.0	8.0	8.3	9.0	9.5	10.0
	Q** = 3.2	4.2	5.2	6.4	7.2	8.2	9.6
0.021	0.05	0.09	0.02	0.03	0.01	0.01	0.01
0.031	0.07	0.11	0.03	0.04	0.02	0.02	0.01
0.042	0.10	0.12	0.05	0.05	0.03	0.03	0.02
0.052	0.14	0.14	0.06	0.06	0.04	0.04	0.02
0.063	0.20	0.17	0.08	0.08	0.04	0.04	0.03
0.073	0.27	0.21	0.10	0.09	0.05	0.05	0.03
0.083	0.39	0.26	0.15	0.10	0.05	0.06	0.04
0.094	0.54	0.36	0.21	0.12	0.06	0.06	0.04
0.104	0.69	0.44	0.28	0.15	0.08	0.08	0.05
0.115	0.82	0.56	0.41	0.21	0.11	0.09	0.06
0.125	0.90	0.68	0.58	0.30	0.16	0.12	0.07
0.135	0.95	0.78	0.69	0.44	0.25	0.16	0.08
0.146	0.97	0.85	0.80	0.55	0.35	0.22	0.10
0.156	0.99	0.91	0.87	0.66	0.48	0.27	0.13
0.167		0.94	0.93	0.77	0.59	0.36	0.19
0.177		0.97	0.96	0.87	0.70	0.48	0.27
0.188		0.99	0.98	0.91	0.80	0.58	0.39
0.198			0.99	0.95	0.86	0.69	0.48
0.208				0.97	0.91	0.78	0.60
0.219				0.99	0.94	0.85	0.71
0.229					0.96	0.90	0.81
0.240					0.98	0.93	0.86
0.250					0.99	0.95	0.90
0.260						0.97	0.93
0.271						0.98	0.95
0.281						0.99	0.96
0.291						0.99	0.97
0.302							0.98
0.312							0.99
0.323							0.99

*Temperatures in degrees Centigrade.

**Discharge in cfs.

TABLE I (Cont.)

CONCENTRATION OF AIR AT VARIOUS DISTANCES FROM THE BED

Run Nos. 151-157
Slope 22.5°

Distance from Channel Bed (ft)	Run - 151	152	153	154	155	156	157
	T* 3.0	3.0	3.0	3.5	3.5	4.0	4.0
	Q** = 3.2	4.2	5.2	6.4	7.2	8.2	9.6
0.021	0.11	0.08	0.07	0.05	0.04	0.04	0.02
0.031	0.14	0.11	0.10	0.07	0.06	0.05	0.04
0.042	0.18	0.13	0.12	0.09	0.08	0.06	0.05
0.052	0.21	0.18	0.13	0.10	0.09	0.07	0.05
0.063	0.26	0.21	0.14	0.11	0.10	0.09	0.06
0.073	0.31	0.21	0.16	0.12	0.11	0.10	0.07
0.083	0.42	0.27	0.19	0.14	0.13	0.11	0.08
0.094	0.52	0.35	0.24	0.17	0.15	0.13	0.09
0.104	0.63	0.46	0.31	0.22	0.17	0.17	0.11
0.115	0.74	0.58	0.42	0.28	0.23	0.21	0.13
0.125	0.84	0.71	0.50	0.37	0.26	0.27	0.14
0.135	0.89	0.80	0.62	0.47	0.37	0.35	0.17
0.146	0.94	0.86	0.70	0.60	0.46	0.45	0.23
0.156	0.96	0.91	0.82	0.69	0.56	0.56	0.27
0.167	0.98	0.95	0.87	0.77	0.68	0.65	0.41
0.177		0.96	0.91	0.85	0.77	0.76	0.51
0.188		0.98	0.94	0.90	0.83	0.82	0.61
0.198		0.99	0.96	0.92	0.88	0.87	0.71
0.208			0.98	0.95	0.92	0.90	0.79
0.219			0.99	0.97	0.95	0.93	0.85
0.229				0.98	0.97	0.95	0.89
0.240				0.99	0.98	0.97	0.93
0.250						0.98	0.95
0.260						0.99	0.97
0.271							0.98
0.281							0.99

*Temperature in degrees Centigrade.

**Discharge in cfs.

TABLE I (Cont.)

CONCENTRATION OF AIR AT VARIOUS DISTANCES FROM THE BED

Run Nos. 171-177
Slope 30°

Distance from Channel Bed (ft)	Run - 171	172	173	174	175	176	177
	T* = 0.9	0.2	0.3	1.7	1.7	0.7	1.2
	Q** = 3.2	4.2	5.2	6.4	7.2	8.2	9.6
0.021	0.13	0.09	0.12	0.09	0.11	0.07	0.02
0.031	0.19	0.12	0.15	0.13	0.14	0.10	0.05
0.042	0.22	0.15	0.18	0.15	0.15	0.12	0.07
0.052	0.28	0.18	0.20	0.17	0.17	0.13	0.09
0.063	0.33	0.22	0.23	0.19	0.20	0.15	0.10
0.073	0.46	0.30	0.26	0.22	0.22	0.17	0.12
0.083	0.57	0.38	0.31	0.25	0.24	0.20	0.15
0.094	0.69	0.50	0.36	0.31	0.28	0.23	0.17
0.104	0.79	0.64	0.44	0.37	0.35	0.26	0.18
0.115	0.87	0.75	0.54	0.46	0.39	0.34	0.25
0.125	0.92	0.84	0.64	0.57	0.47	0.39	0.29
0.135	0.96	0.89	0.73	0.65	0.58	0.48	0.35
0.146	0.98	0.92	0.80	0.72	0.64	0.55	0.45
0.156		0.95	0.85	0.79	0.73	0.66	0.53
0.167		0.98	0.90	0.84	0.79	0.74	0.66
0.177		0.99	0.94	0.89	0.86	0.79	0.73
0.188			0.96	0.94	0.89	0.86	0.79
0.198			0.98	0.96	0.93	0.89	0.85
0.208			0.99	0.98	0.95	0.93	0.87
0.219				0.99	0.96	0.95	0.91
0.229					0.98	0.96	0.95
0.240					0.99	0.97	0.96
0.250						0.98	0.97
0.260						0.99	0.98
0.271							0.99

*Temperature in degrees Centigrade.

**Discharge in cfs.

TABLE I (Cont.)

CONCENTRATION OF AIR AT VARIOUS DISTANCES FROM THE BED

Run Nos. 181-187
Slope 37.5°

Distance from Channel Bed (ft)	Run - 181	182	183	184	185	186	187
	T* = 1.0	0.4	0.4	0.8	0.8	0.5	0.2
	Q** = 3.2	4.2	5.2	6.4	7.2	8.2	9.6
0.021	0.23	0.21	0.20	0.17	0.13	0.12	0.10
0.031	0.26	0.23	0.21	0.19	0.14	0.13	0.09
0.042	0.30	0.26	0.23	0.19	0.15	0.14	0.10
0.052	0.37	0.30	0.26	0.22	0.17	0.15	0.11
0.063	0.47	0.33	0.29	0.24	0.19	0.17	0.11
0.073	0.60	0.41	0.33	0.27	0.22	0.20	0.13
0.083	0.68	0.49	0.37	0.31	0.25	0.22	0.14
0.094	0.77	0.55	0.45	0.36	0.30	0.25	0.18
0.104	0.85	0.67	0.52	0.43	0.36	0.30	0.22
0.115	0.90	0.77	0.61	0.50	0.42	0.37	0.25
0.125	0.94	0.83	0.66	0.56	0.52	0.46	0.30
0.135	0.96	0.87	0.75	0.66	0.62	0.54	0.37
0.146	0.98	0.92	0.82	0.72	0.68	0.59	0.45
0.156	0.99	0.95	0.87	0.80	0.77	0.70	0.57
0.167		0.97	0.92	0.85	0.83	0.77	0.60
0.177		0.98	0.94	0.86	0.86	0.83	0.71
0.188		0.99	0.96	0.93	0.90	0.87	0.76
0.198			0.97	0.95	0.93	0.91	0.84
0.208			0.98	0.96	0.95	0.92	0.88
0.219			0.99	0.97	0.96	0.95	0.90
0.229				0.98	0.98	0.96	0.93
0.240				0.99	0.99	0.98	0.95
0.250						0.99	0.96
0.260							0.97
0.271							0.98
0.281							0.99

*Temperature in degrees Centigrade.

**Discharge in cfs.

TABLE I (Cont.)

CONCENTRATION OF AIR AT VARIOUS DISTANCES FROM THE BED

Run Nos. 191-197
Slope 45°

Distance from Channel Bed (ft)	Run - 191	192	193	194	195	196	197
	T* = 2.0	2.0	2.0	1.5	2.0	2.5	2.0
	Q** = 3.2	4.2	5.2	6.4	7.2	8.2	9.6
0.021	0.32	0.29	0.28	0.20	0.19	0.16	0.08
0.031	0.36	0.32	0.31	0.22	0.20	0.17	0.08
0.042	0.40	0.34	0.32	0.25	0.21	0.18	0.09
0.052	0.44	0.38	0.34	0.26	0.23	0.20	0.10
0.063	0.51	0.42	0.37	0.28	0.26	0.23	0.13
0.073	0.58	0.47	0.42	0.31	0.29	0.25	0.15
0.083	0.66	0.54	0.46	0.35	0.32	0.28	0.17
0.094	0.74	0.61	0.51	0.42	0.36	0.31	0.20
0.104	0.81	0.68	0.58	0.45	0.41	0.36	0.23
0.115	0.86	0.76	0.65	0.53	0.46	0.41	0.27
0.125	0.91	0.82	0.73	0.63	0.53	0.48	0.33
0.135	0.94	0.86	0.78	0.72	0.58	0.55	0.39
0.146	0.96	0.91	0.83	0.76	0.65	0.62	0.48
0.156	0.98	0.94	0.87	0.83	0.75	0.72	0.55
0.167	0.99	0.96	0.91	0.87	0.81	0.76	0.63
0.177		0.97	0.94	0.90	0.86	0.82	0.71
0.188		0.98	0.96	0.93	0.90	0.86	0.77
0.198		0.99	0.97	0.95	0.93	0.89	0.84
0.208			0.98	0.96	0.95	0.92	0.88
0.219			0.99	0.98	0.97	0.94	0.91
0.229				0.99	0.98	0.96	0.94
0.240					0.99	0.97	0.96
0.250						0.98	0.97
0.260						0.98	0.98
0.271						0.99	0.99

*Temperature in degrees Centigrade.

**Discharge in cfs.

concentration meter probes. The position of the measurement is given in feet normal to the channel bottom. As seen from Fig. 4, the air concentration increases continuously from the concentration near the bed. The concentration increases slowly in the lower region near the bed, more rapidly in the central portion, and then more slowly in the upper region, appearing to approach 100 per cent air concentration asymptotically. In the upper regions the curves are very similar in appearance for all flow conditions, while the air concentration near the bed appears to depend upon the discharge and slope. Although there is no clear line of demarcation in the two regions, this distribution tends to support the suggestion that has been made--that in the lower portion of the stream air bubbles are mixed or suspended in water, while the upper region consists of water particles projected into the atmosphere. The existence of these water droplets can be confirmed by holding ones hand just above the main flow. It is apparent from these plots, as typified by Fig. 4, that the two portions of the complete curve have different characteristics.

B. Depth of Flow

It is apparent from Fig. 4 and Figs. B-1 to B-7 in Appendix B, showing the distribution of air concentration as a function of distance from the bed, that there is no definite upper boundary to the flow. Under these conditions several different depth parameters related to the air distribution may be defined, each having application for specific purposes.

1. A mean depth $\bar{d}$ representing a mean depth of flow or the depth of flow if all of the entrained air were removed may be defined as

$$\bar{d} = \int_0^\infty (1 - C)\, dy \qquad (1)$$

where y is the normal distance from the bed and C is the concentration of air as a function of y.

2. If the air concentration is plotted as a probability function of the depth (see Appendix A and Fig. A-10), it is seen that the data fit such a curve remarkably well. An upper boundary of the flow may be defined on this basis, as the value of y where the

air concentration has any arbitrarily prescribed value as given by a fitted line through the points. For some purposes such as computing the mean air concentration, it is convenient to define this upper limit, d_u, as that value of y where the air concentration, C, is 0.99. Other depths may be similarly defined such as, d_{50} is that value of y where $C = 0.50$.

3. A depth has been defined as that corresponding to that distance y where the air concentration is $C = 0.95$ [5]. This depth was chosen arbitrarily as a depth where the concentration of air is reliably measured, and which includes from 98 to 99 per cent of all of the water. This represents essentially the maximum distance from the bed where water will be found.

The measured or computed depths for each run have been tabulated in Table II, Columns 8 to 10.

The depth parameters, thus determined from the experimental data for each run, have been plotted in terms of the total water discharge for each slope in Figs. 5 to 7. The mean depth $\bar{d}$ (Fig. 5) increases with the discharge and decreases with the slope. In Fig. 6 d_u has been similarly plotted. Here again the depth, d_u, or essentially the maximum height to which water particles are carried above the bed, increases with the discharge, but is much less dependent upon the slope. It is apparent in Fig. 7 that the depth where the concentration is 0.5, $d_{0.50}$ is very similar to the plots of $\bar{d}$. In general, $d_{0.50}$ is slightly larger than $\bar{d}$. The difference between $\bar{d}$ and $d_{0.50}$ is a measure of the nonsymmetry of the air-concentration distribution.

C. Air Concentration

The concentration of air in the flow varies from some value near the bed to 100 per cent air at some elevation above the bed. The definition of mean air concentration is then somewhat arbitrary, and depends upon the choice of the upper limit. Further, in the lower portions of the flow the air is in the form of bubbles of air suspended in water, while in the upper portions of the flow the high air concentrations suggest the presence of water droplets surrounded by air. Since the air concentration approaches 100 per cent asymptotically, the upper limit of the flow can be defined as the depth

TABLE II - CHARACTERISTICS OF AIR-ENTRAINED FLOWS (EXPERIMENTAL DATA)

(1) Run No.	(2) Date	(3) Temp. °C	(4) Sta. ft	(5) Slope α Deg.	(6) Disch. Q cfs	(7) d_e ft	(8) d_u ft
161	3-5-54	0.2	48	7.5	3.2	0.075	0.165
162	3-5-54	0.2			4.2	0.086	0.198
163	3-5-54	0.2			5.2	0.122	0.216
164	3-5-54	0.2			6.4	0.141	0.245
165	3-5-54	1.0			7.2	0.162	0.258
166	3-10-54	1.3			8.2	0.178	0.279
167	3-12-54	0.3			9.6	0.205	0.311
141	4-9-54	5.5	45	15.0	3.2	0.055	0.154
142	4-12-54	7.0			4.2	0.064	0.187
143	4-13-54	8.0			5.2	0.097	0.192
144	4-13-54	8.3			6.4	0.128	0.217
145	4-13-54	9.0			7.2	0.145	0.243
146	4-15-54	9.5			8.2	0.164	0.275
147	4-19-54	10.0			9.6	0.190	0.284
151	4-6-54	3.0	45	22.5	3.2	0.055	0.171
152	4-6-54	3.0			4.2	0.075	0.190
153	4-6-54	3.0			5.2	0.095	0.213
154	4-6-54	3.5			6.4	0.121	0.232
155	4-6-54	3.5			7.2	0.140	0.246
156	4-8-54	4.0			8.2	0.158	0.247
157	4-8-54	4.0			9.6	0.175	0.272
171	3-13-54	0.8	45	30.0	3.2	0.060	0.156
172	3-15-54	0.2			4.2	0.080	0.184
173	3-15-54	0.3			5.2	0.095	0.211
174	3-16-54	1.7			6.4	0.123	0.223
175	3-16-54	1.7			7.2	0.130	0.240
176	3-17-54	0.7			8.2	0.155	0.251
177	3-17-54	1.2			9.6	0.190	0.259
181	3-25-54	1.0	44	37.5	3.2	0.070	0.153
182	3-25-54	0.4			4.2	0.090	0.186
183	3-25-54	0.4			5.2	0.110	0.217
184	3-25-54	0.8			6.4	0.135	0.233
185	3-25-54	0.8			7.2	0.160	0.239
186	3-25-54	0.5			8.2	0.175	0.247
187	3-25-54	0.2			9.6	0.226	0.262
191	3-26-54	2.0	43	45.0	3.2	0.076	0.171
192	3-26-54	2.0			4.2	0.096	0.195
193	3-26-54	2.0			5.2	0.114	0.220
194	3-26-54	1.5			6.4	0.156	0.232
195	3-26-54	2.0			7.2	0.174	0.242
196	3-26-54	2.5			8.2	0.210	0.260
197	3-29-54	2.0			9.6	0.285	0.268

TABLE II - CHARACTERISTICS OF AIR-ENTRAINED FLOWS (EXPERIMENTAL DATA) (Cont.)

Run No.	(9) d_{50} ft	(10) $\bar{d}$ ft	(11) $\frac{q}{S^{1/2}}$	(12) $\bar{c}$	(13) $\frac{S}{q^{2/3}}$	(14) $\bar{V}$ fps	(15) $V_* = \sqrt{g \bar{d} \sin \alpha}$	(16) $\frac{\bar{V}}{V_*}$
161	0.119	0.116	5.92	0.296	0.0790	18.3	0.699	26.2
162	0.141	0.138	7.76	0.302	0.0655	20.3	0.763	26.6
163	0.156	0.155	9.60	0.281	0.0570	22.3	0.808	27.6
164	0.178	0.173	11.83	0.294	0.0495	24.7	0.853	29.0
165	0.192	0.188	13.30	0.272	0.0460	25.5	0.889	28.7
166	0.213	0.208	15.14	0.255	0.0420	26.3	0.936	28.1
167	0.232	0.227	17.75	0.271	0.0380	28.2	0.977	28.9
141	0.091	0.086	4.20	0.440	0.1570	24.8	0.848	29.3
142	0.109	0.102	5.52	0.456	0.1300	27.5	0.921	29.9
143	0.120	0.117	6.83	0.389	0.1130	29.5	0.989	29.9
144	0.142	0.136	8.40	0.371	0.0985	31.3	1.066	29.4
145	0.160	0.156	9.45	0.357	0.0915	30.7	1.142	26.9
146	0.178	0.175	10.76	0.365	0.0835	31.3	1.207	25.9
147	0.199	0.196	12.60	0.311	0.0750	32.7	1.277	25.6
151	0.091	0.085	3.45	0.501	0.2320	25.0	1.025	24.4
152	0.105	0.100	4.53	0.472	0.1925	27.8	1.112	25.0
153	0.122	0.116	5.56	0.454	0.1670	29.8	1.197	24.9
154	0.137	0.131	6.91	0.434	0.1460	32.5	1.272	25.5
155	0.148	0.142	7.77	0.424	0.1345	33.9	1.321	25.6
156	0.150	0.145	8.84	0.413	0.1235	37.7	1.337	28.2
157	0.176	0.170	10.35	0.374	0.1110	37.6	1.449	26.0
171	0.078	0.072	3.02	0.539	0.3030	29.6	1.075	27.5
172	0.095	0.088	3.96	0.522	0.2510	31.8	1.190	26.7
173	0.110	0.101	4.90	0.520	0.2180	34.2	1.277	26.8
174	0.118	0.111	6.05	0.501	0.1900	38.3	1.338	28.6
175	0.125	0.118	6.80	0.510	0.1755	40.8	1.376	29.6
176	0.137	0.130	7.74	0.483	0.1615	42.1	1.445	29.2
177	0.152	0.145	9.06	0.438	0.1450	44.0	1.530	28.8
181	0.065	0.061	2.74	0.602	0.3700	35.1	1.092	32.1
182	0.084	0.078	3.60	0.580	0.3065	35.8	1.237	29.0
183	0.098	0.092	4.45	0.575	0.2660	37.6	1.344	28.0
184	0.112	0.105	5.48	0.548	0.2320	40.5	1.438	28.2
185	0.123	0.114	6.16	0.522	0.2140	42.0	1.496	28.1
186	0.131	0.123	7.01	0.503	0.1970	44.5	1.551	28.7
187	0.151	0.143	8.23	0.453	0.1770	44.7	1.675	26.6
191	0.063	0.058	2.54	0.662	0.4290	36.9	1.215	30.4
192	0.077	0.071	3.33	0.636	0.3550	39.5	1.346	29.3
193	0.092	0.082	4.12	0.627	0.3085	42.3	1.446	29.2
194	0.108	0.098	5.08	0.578	0.2685	43.6	1.581	27.6
195	0.118	0.108	5.71	0.554	0.2480	44.4	1.660	26.8
196	0.127	0.117	6.50	0.548	0.2280	46.5	1.732	26.8
197	0.148	0.141	7.61	0.474	0.2050	45.5	1.895	24.2

TABLE II - CHARACTERISTICS OF AIR-ENTRAINED FLOWS (EXPERIMENTAL DATA) (Cont.)

Run No.	(17) $\frac{V_*}{(\bar{d})^{5/4}}$	(18) $\frac{q_1}{q}$	(19) $\times 10^{-5}$ Re	(20) f	(21) $\frac{h}{d_{50}}$	(22) z	(23) C_o
161	10.28	0.928	4.46	0.01166	0.237	1.350	0.017
162	9.09	0.925	5.86	0.01140	0.261	1.120	0.026
163	8.33	0.933	7.26	0.01050	0.326	1.625	0.010
164	7.69	0.925	8.93	0.00955	0.222	1.185	0.020
165	7.17	0.935	10.22	0.00973	0.221	1.545	0.011
166	6.69	0.936	11.82	0.01014	0.199	1.180	0.017
167	6.27	0.935	13.40	0.00960	0.217	1.386	0.012
141	18.23	0.862	5.30	0.00936	0.435	0.691	0.113
142	15.90	0.826	7.27	0.00898	0.467	0.433	0.158
143	14.32	0.883	9.24	0.00898	0.363	0.822	0.075
144	12.63	0.888	11.50	0.00928	0.329	0.620	0.088
145	11.66	0.906	13.15	0.01106	0.327	1.053	0.042
146	10.67	0.895	15.28	0.01189	0.334	0.763	0.065
147	9.82	0.910	18.17	0.00975	0.270	0.843	0.046
151	22.30	0.805	4.87	0.01343	0.529	0.427	0.184
152	19.90	0.823	6.40	0.01280	0.499	0.418	0.165
153	17.60	0.842	7.93	0.01285	0.441	0.410	0.150
154	16.12	0.857	9.91	0.01229	0.423	0.488	0.125
155	15.20	0.865	11.18	0.01220	0.401	0.506	0.122
156	14.86	0.871	12.94	0.01007	0.396	0.576	0.109
157	13.29	0.888	15.15	0.01185	0.329	0.615	0.085
171	29.10	0.780	4.51	0.01053	0.617	0.353	0.207
172	24.80	0.820	5.86	0.01119	0.566	0.390	0.207
173	22.60	0.787	7.26	0.01113	0.552	0.332	0.208
174	20.90	0.807	9.37	0.00975	0.540	0.358	0.184
175	19.95	0.798	10.55	0.00908	0.565	0.357	0.194
176	18.52	0.820	11.58	0.00941	0.526	0.416	0.165
177	17.00	0.858	13.84	0.00967	0.428	0.504	0.124
181	36.45	0.725	4.69	0.00776	0.827	0.223	0.270
182	29.90	0.727	5.89	0.00951	0.741	0.231	0.262
183	26.40	0.743	7.29	0.01021	0.721	0.182	0.258
184	24.00	0.760	9.03	0.01005	0.670	0.272	0.230
185	22.70	0.800	10.17	0.01013	0.575	0.378	0.192
186	21.30	0.800	11.51	0.00971	0.540	0.310	0.185
187	19.03	0.833	13.40	0.01125	0.487	0.480	0.141
191	42.60	0.638	4.74	0.00865	1.054	0.145	0.360
192	36.90	0.655	6.22	0.00926	0.937	0.131	0.343
193	32.90	0.668	7.70	0.00935	0.768	0.155	0.333
194	29.00	0.729	9.32	0.01050	0.707	0.211	0.270
195	26.80	0.740	10.68	0.01120	0.648	0.222	0.251
196	25.30	0.755	12.28	0.01112	0.634	0.259	0.232
197	21.70	0.825	14.23	0.01390	0.496	0.487	0.150

where the air concentration is some specified value. If the upper limit of the flow is defined as, d_u, that depth where the air concentration is 0.99 or the water concentration is 0.01, the mean air concentration is then

$$\bar{C} = 1/d_u \int_0^{d_u} C dy \qquad (2)$$

The mean air concentration as computed from the concentration data is plotted in Fig. 8 in terms of the discharge for each slope. The mean air concentration increases with the slope and decreases with the discharge.

IV. ANALYSIS OF EXPERIMENTAL DATA

A. Relation Between Depth of Flow, Discharge, and Slope

The effective depth of flow in self-aerated high-velocity flows is presumably the transition depth between the upper regions consisting of water particles or droplets in air, and the lower region made up of air bubbles in water. The distribution mechanism appears to be different in the two regions (see Appendix A). The analysis of the flow hinges upon the definition of the transition depth. The so-called mean depth, $\bar{d}$, may be used as a measure of the depth for purposes of bulk flow conditions.

The mean depth, $\bar{d}$, plotted in Fig. 5, shows that $\bar{d}$ increases with discharge, and decreases with slope. If the resistance to flow for aerated flow is related to the discharge and slope, in a manner similar to that of unaerated flow, the mean depth should be related to the discharge and the square root of the slope. The mean depth, $\bar{d}$, as computed from the air-concentration measurements has been plotted logarithmically in Fig. 9 as a function of $q/S^{1/2}$, (Column 11, Table II) where q is the unit water discharge and S is the sine of the slope angle α. All of the points cluster about a single straight line, the slope of which is two-thirds. For the two-dimensional case this implies that the Chezy roughness coefficient is a constant, and the variables are related by

$$q = 160\ (\bar{d})^{3/2}\ S^{1/2} \qquad (3)$$

A similar curve is obtained when d_{50} is plotted as a function of $q/S^{1/2}$ as in Fig. 10.

In order to compare these results with those obtained for unaerated flow in the same channel, a series of measurements were made for lesser slopes such that the flow would be unaerated. In Fig. 11 the measured depths for unaerated flow are plotted in the same manner as a function of $q/S^{1/2}$, where it is seen that these data fit essentially on a single straight line whose slope is also two-thirds. The measured depths for unaerated flow are in all cases larger than $\bar{d}$ for the same value of $q/S^{1/2}$.

Since the unaerated flow is homogeneous with known fluid properties, it can be treated in the usual manner. In Fig. 12 the friction factor f has been plotted in terms of the Reynolds number, where the terms are defined as follows:

$$f = 8\left(\frac{gRS}{(\bar{V})^2}\right) \tag{4}$$

and

$$Re = \frac{4\bar{V}R}{\nu} \tag{5}$$

In Eqs. (4) and (5) in addition to terms previously defined, R is the hydraulic radius of the flow, g is the acceleration due to gravity, and ν is the kinematic viscosity of the water. The data fall very closely to the f - Re curve for smooth pipes as defined by the Kármán-Nikuradse curve.

Aerated flow, on the other hand, is characterized by an indefinite depth of flow and the property of nonhomogeneity because of the presence of air in varying amounts with respect to distance from the bed. Consequently, the kinematic viscosity, and hence the Reynolds number is undefined.

For purposes of comparison however, the friction factor, f, (Table II, Column 20) based upon the mean depth $\bar{d}$ and the mean velocity, $q/(\bar{d})$, as in Eq. (4), was computed and plotted in Fig. 13. The Reynolds number was computed on the basis of Eq. (5) using the mean depth and the kinematic viscosity for the water alone. The computed points all lie well below the data

obtained for the unaerated flow in the same channel. The data for unaerated flow correspond closely to results obtained for so-called hydrodynamically smooth surfaces. The values of f computed for aerated flow fall below this line and indicate that either or both, (1) the effective depth is greater than $\bar{d}$, and (2) the kinematic viscosity of aerated flow is less than that for unaerated flow, since the curve for hydrodynamically smooth surfaces represents the lowest values of f.

For this particular channel and experimental data, a qualitative comparison can be made on an empirical basis. The equation of the line representing the relationship of d_m and $q/S^{1/2}$ shown in Fig. 11 is

$$q = 112.5\ d_m^{3/2}\ S^{1/2} \tag{6}$$

or

$$\bar{V} = 112.5\ d_m^{1/2}\ S^{1/2} \tag{7}$$

where d_m is the mean depth of unaerated flow. For the range of data considered, the coefficient 112.5 is a constant and corresponds to a Chezy coefficient. If it is assumed that this constant is a characteristic of the channel surface and applied also to aerated flow, Eq. (7) may be used to calculate the effective depth of the aerated flow since

$$\bar{V} = q/(\bar{d})$$

where $\bar{d}$ is the area per unit width occupied by water. Consequently,

$$\frac{q}{\bar{d}} = 112.5\ d_a^{1/2}\ S^{1/2} \tag{8}$$

where d_a is some effective depth for the aerated flow. This curve has been plotted in Fig. 14 showing d_a as a function of $q/(\bar{d})S^{1/2}$. The value of d_u, as measured for the aerated flow, has also been plotted in Fig. 14 in terms of $q/(\bar{d})S^{1/2}$ for purposes of comparison. It is apparent that for some series d_a is somewhat less than d_u and that for the 7.5- and 15-degree series, d_a

is greater than d_u. It would be expected that the computed effective depth would be considerably less than d_u, since d_u includes practically all of the spray. This suggested rather strongly that the resistance coefficient for aerated flow is considerably less than that for unaerated flow. A direct comparison of Eqs. (3) and (6) indicates that the resistance of aerated flow is only 70 per cent of that for unaerated flow.

B. Relation Between Air Concentration, Discharge, and Slope

The air-concentration distribution graphs shown in Fig. 4 and Figs. B-1 to B-7 are tentatively analyzed in Appendix A. Aside from the actual distribution of the air concentration, probably the most significant concentration characteristic is the mean air concentration in the flow as a whole. These data were shown in Fig. 10 as a function of the water discharge. In Fig. 15 the mean air concentration has been replotted empirically in terms of $S/q^{2/3}$. The data appear to fall on a single curve for the lower values of $S/q^{2/3}$, but the data for each slope leaves the common curve at the higher values of $S/q^{2/3}$ approaching separate upper asymptotes.

The parameter $S/q^{2/3}$ can be written in an alternate form that provides a greater insight into the mechanism of air-entrained flow by introducing the shear velocity and the depth. The slope can be written in terms of the shear velocity defined as

$$S = \frac{V_*^2}{g\bar{d}} \tag{9}$$

and from Eq. (3)

$$q = k\, g^{1/2} (\bar{d})^{3/2} S^{1/2} \tag{3}$$

From Eqs. (3) and (9)

$$\frac{S}{q^{2/3}} = \left(\frac{V_*}{k^{1/2}\, g^{3/4}\, (\bar{d})^{5/4}} \right)^{4/3}$$

The mean air concentration has been plotted in terms of $V_*/(\bar{d})^{5/4}$ in Fig. 16,

where, as expected, the points show trends for all of the experimental data as in Fig. 15. The intensity of turbulent mixing throughout the fluid would appear to depend upon the shear velocity, but as the depth increases the violence of agitation near the surface is progressively damped out. Consequently, it is expected that the mean air concentration would increase with V_* and decrease with the depth. This relationship is indicated in Fig. 16, where the mean air concentration increases with an increase in the parameter $V_*/(\bar{d})^{5/4}$.

The proportion of the total water discharge that occurs in the region below $\bar{d}$ is related to the mean air concentration, and can be approximated by

$$\frac{q_1}{q} = \frac{\bar{d}}{d_u}\left(\frac{1 - \bar{C}_1}{1 - \bar{C}}\right) \qquad (10)$$

where, in addition to the variables previously defined, q_1 is the water discharge in the region between the lower boundary and $\bar{d}$, and $\bar{C}_1$ is the mean air concentration in this region. This ratio has been plotted in Fig. 17 as a function of $S/q^{2/3}$ which shows the development of a family of curves as the data for each slope departs from the common curve. It is interesting to note that for small values of the parameter $S/q^{2/3}$, over 90 per cent of the water discharge is below $\bar{d}$, while for high values this ratio drops to about 60 per cent. Presumably when the slope approaches zero or the discharge becomes very large, the air entrainment approaches zero as $\bar{d}$ approaches the actual depth, and the ratio q_1/q approaches 1.0.

V. SUMMARY AND CONCLUSIONS

The experiments reported here consisted of the measurement of the air-concentration distribution profile for self-aerated high-velocity open-channel flows at discharges ranging from 3.2 to 9.6 cfs on slopes ranging from 7.5 to 45 degrees in a painted-steel channel 1.5-ft wide. The results of the experiments are presented in tabular form in Tables I and II, and in the form of air-concentration distribution curves in Figs. B-1 to B-7 in Appendix B.

The results of the experiments may be summarized as follows:

1. The typical air-concentration distribution curve appeared to be made up of two parts; a lower portion near the bed consisting

of air bubbles surrounded by water, and an upper portion consisting of water particles in the atmosphere with a transition zone with a high concentration gradient separating the two regions (see Appendix A).

2. The upper boundary of an air-entrained flow is indefinite, and its definition is to a certain extent arbitrary. A mean depth $\bar{d}$, based upon the air concentration distribution and the depth corresponding to $C = 0.5$, may be correlated with the water discharge and slope.

3. The Darcy f computed on the basis of the mean depth $\bar{d}$ is less than that for smooth surfaces as given by the f - Re curve when the Reynolds number is computed on the basis of the kinematic viscosity for the water. Possible explanations are either or both of (1) the effective depth is greater than $\bar{d}$, or (2) the effective kinematic viscosity of the air-water mixture is less than that for water alone. Plotting $\bar{d}$ as a function of $q/S^{1/2}$ indicated that the resistance coefficient is a constant and thus independent of the Reynolds number. The value of the coefficient using the mean depth, $\bar{d}$, is approximately 70 per cent of that for unaerated flow in the same channel. If the effective depth is assumed to be that corresponding to d_u (the depth where $C = 0.99$), the roughness coefficient is about equal to that for unaerated flow.

4. It was found that the mean air concentration in the flow was a function of $S/q^{2/3}$, which for these data is related to $V_*/(\bar{d})^{5/4}$. This suggests that the intensity of the turbulent fluctuations causing air entrainment are increasingly damped with increasing depth.

5. The proportion of the total flow taking place in the region below $\bar{d}$ decreases from over 90 per cent for small values of $S/q^{2/3}$, to approximately 60 per cent for the highest values of $S/q^{2/3}$ measured in these experiments.

BIBLIOGRAPHY

[1] Lamb, Owen P. Air Entrainment in Flowing Water, A Summary and Bibliography of Literature. University of Minnesota, St. Anthony Falls Hydraulic Laboratory Project Report No. 19, August 1949. 41 pages.

[2] Lamb, Owen P. An Experimental Channel for the Study of Air Entrainment in High-Velocity Flow. University of Minnesota, St. Anthony Falls Hydraulic Laboratory Project Report No. 34, November 1952. 41 pages.

[3] Lamb, Owen P. and Killen, John M. An Electrical Method for Measuring Air Concentration in Flowing Air-Water Mixtures. University of Minnesota, St. Anthony Falls Hydraulic Laboratory Technical Paper No. 2, Series B, March 1950. 36 pages.

[4] Straub, Lorenz G., Killen, John M., and Lamb, Owen P. Velocity Measurement of Air-Water Mixtures. University of Minnesota, St. Anthony Falls Hydraulic Laboratory Technical Paper No. 10, Series B, March 1952. 28 pages.

[5] Straub, Lorenz G. and Lamb, Owen P. "Experimental Studies of Air Entrainment in Open Channel Flow." Proceedings of the Minnesota International Hydraulic Convention, pp. 425-437. September 1-4, 1953.

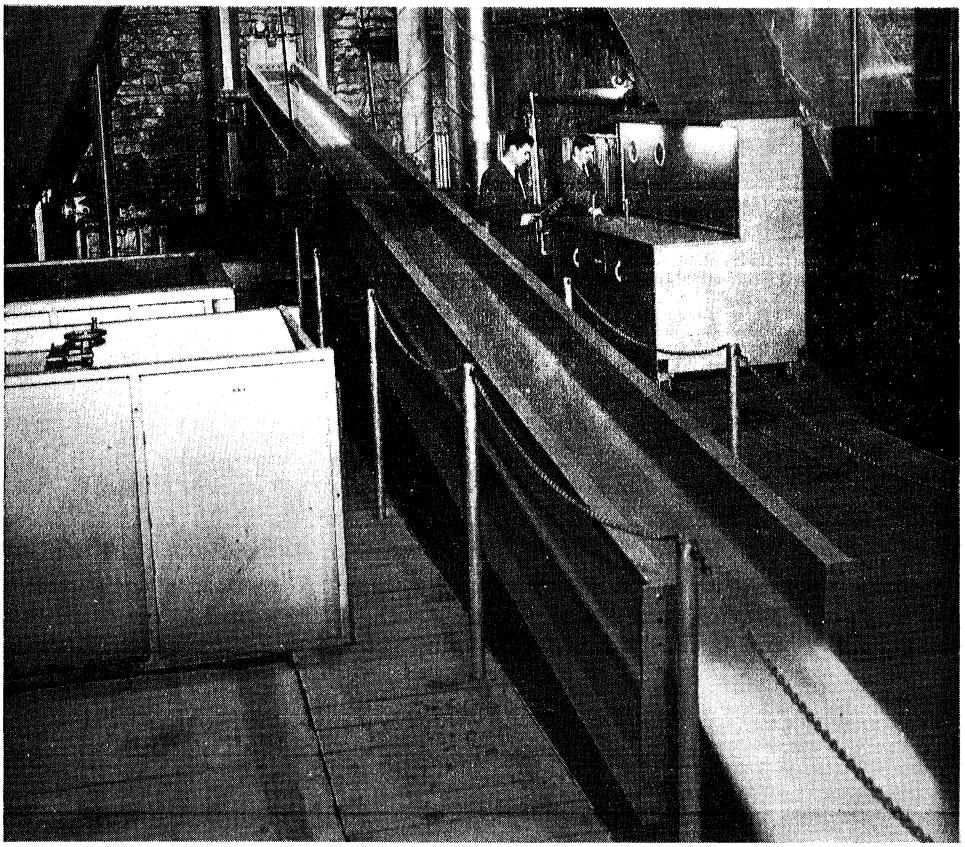

Fig. 1 - General View of Channel for Air-Entrainment Experiments

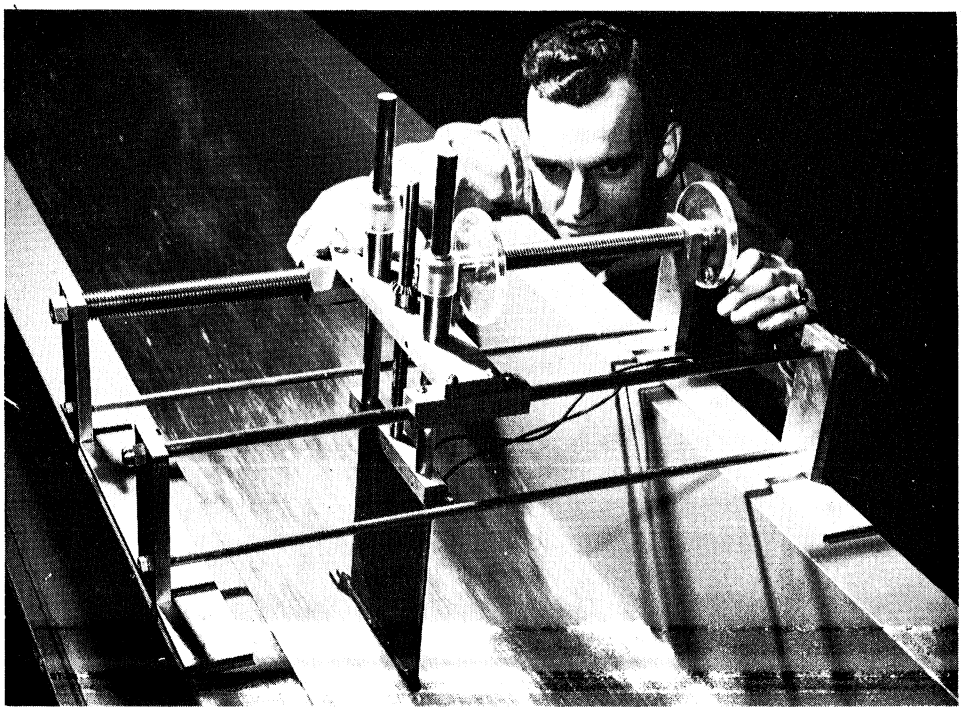

Fig. 2 - Air-Concentration Meter Used in High-Velocity Flow

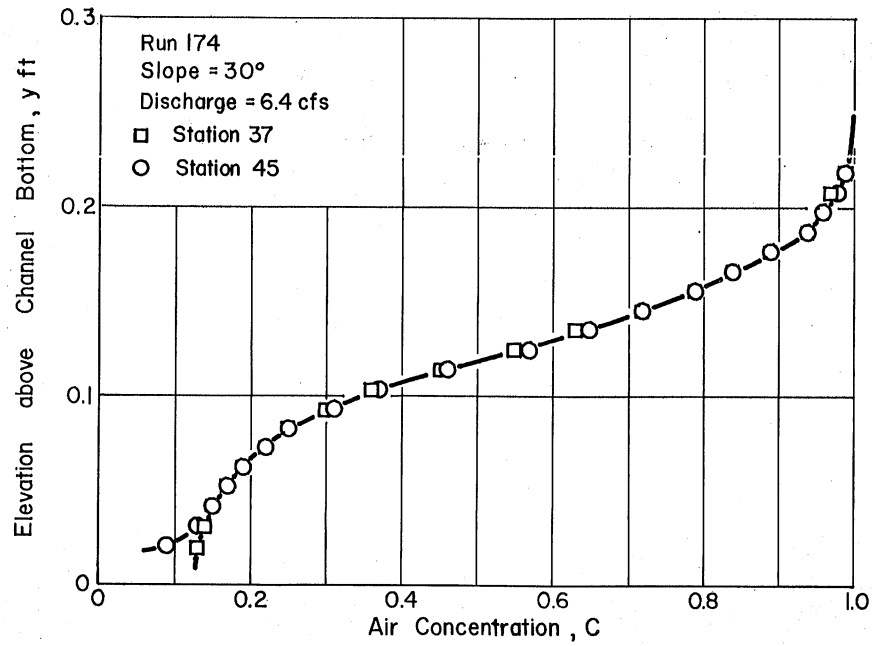

Fig. 3 – Example of Differences in Air-Concentration Profiles

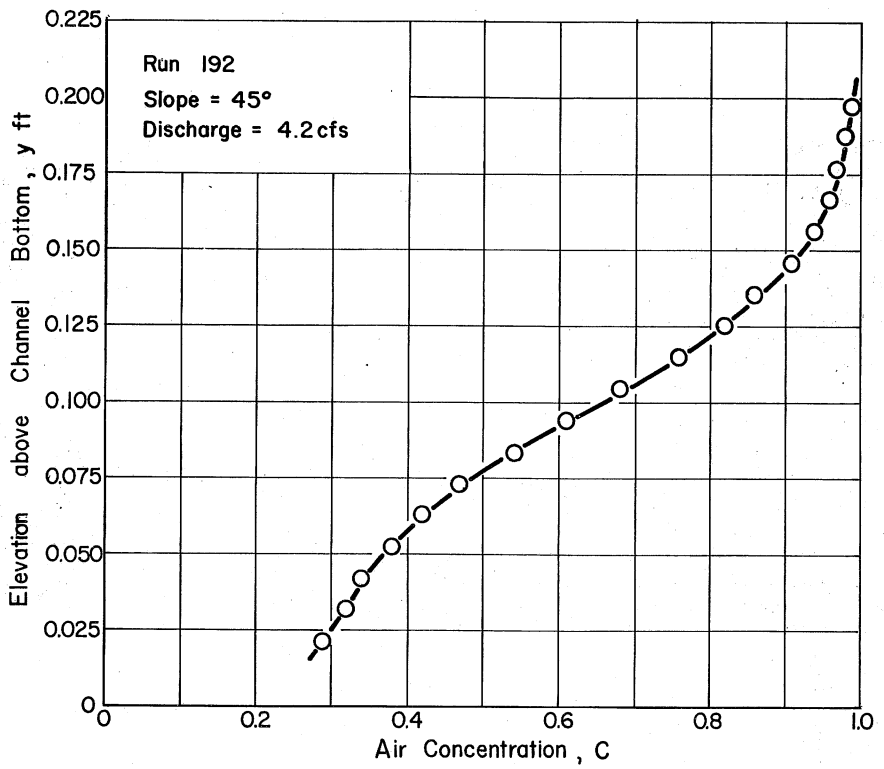

Fig. 4 – Typical Experimental Concentration Distribution

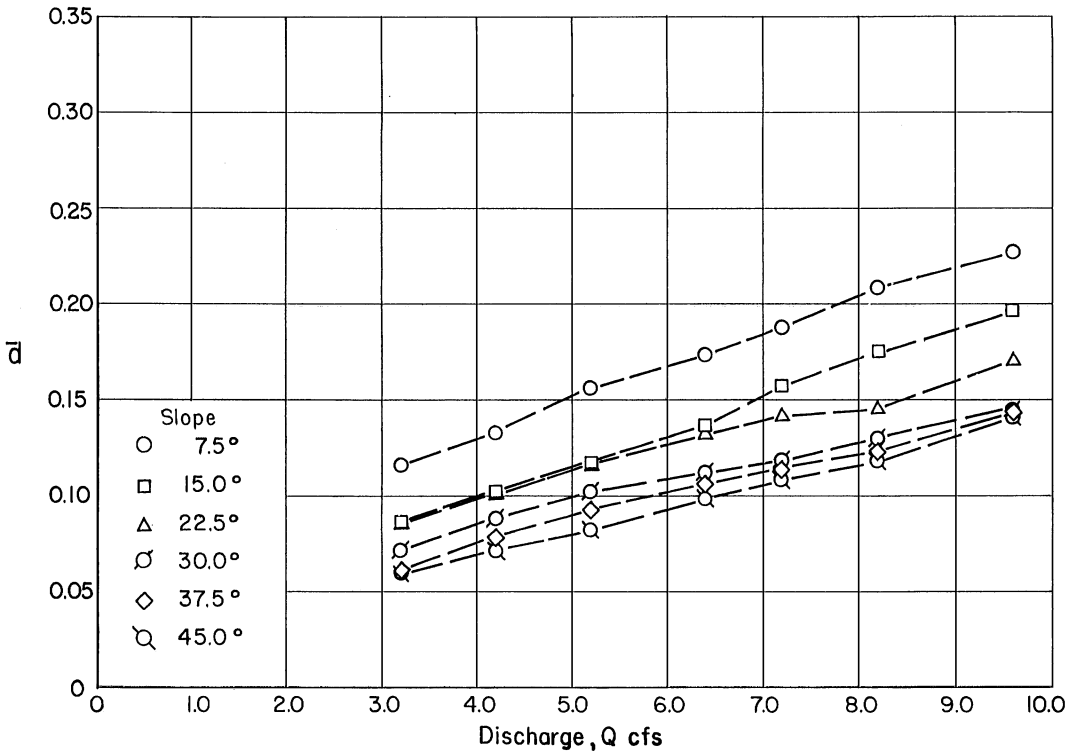

Fig. 5 – Mean Depth as a Function of Discharge

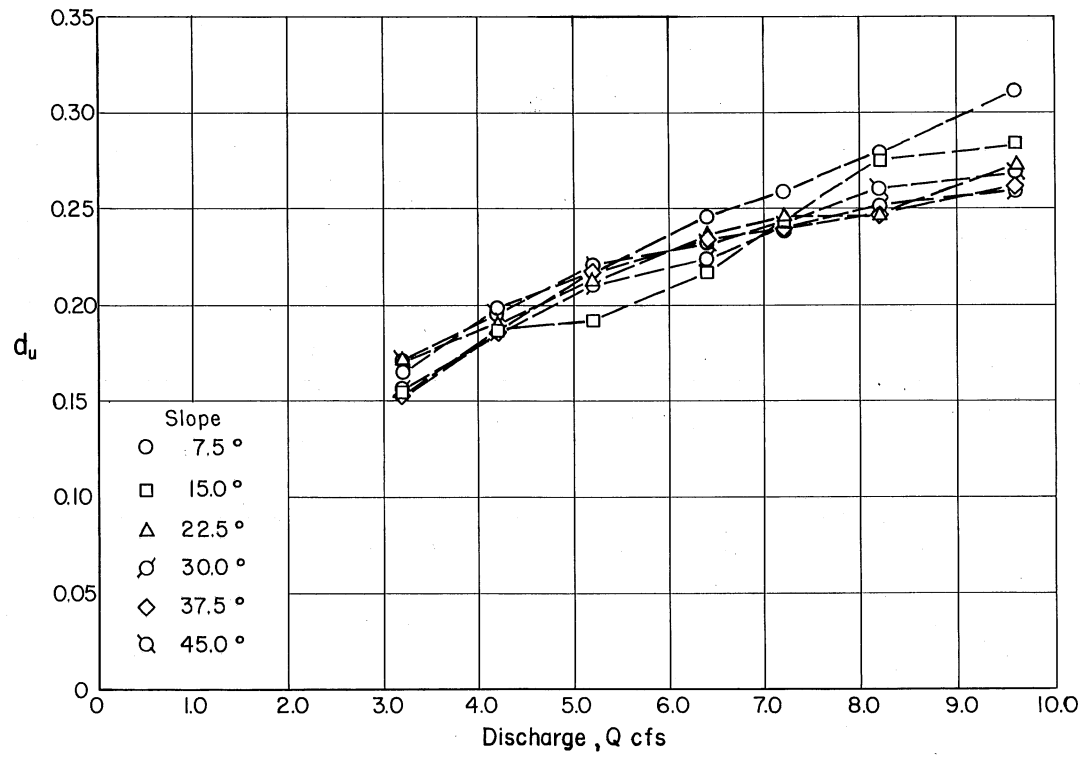

Fig. 6 – Maximum Depth as a Function of Discharge

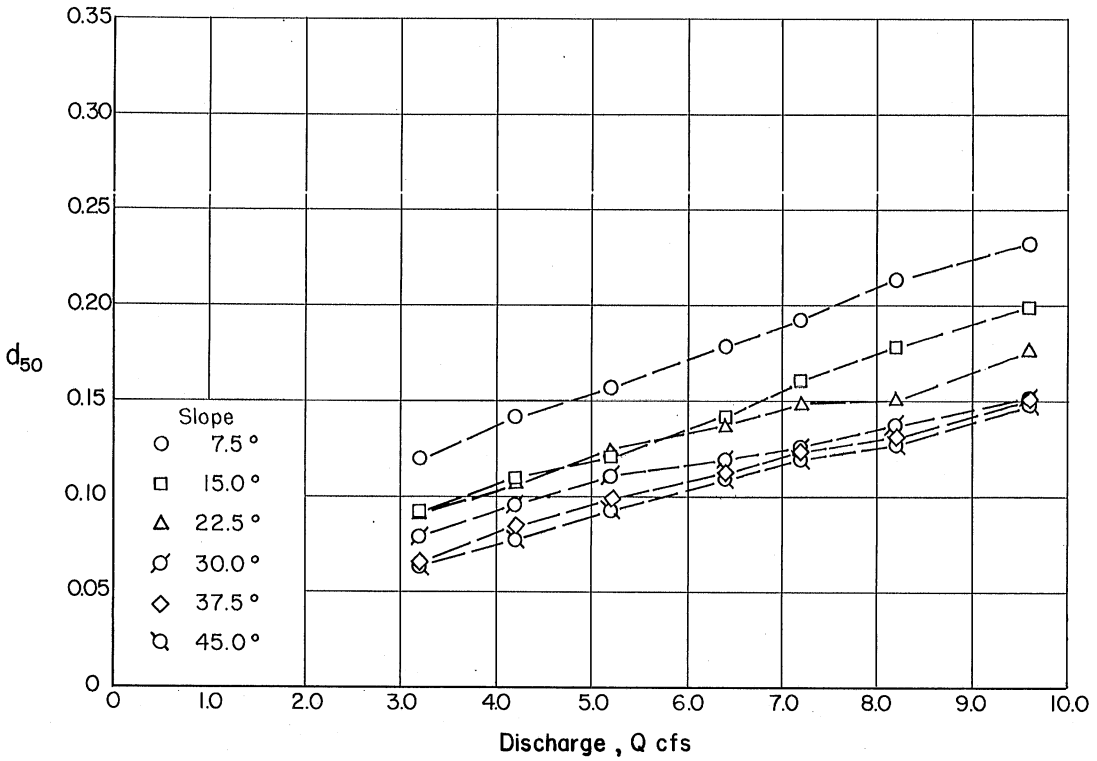

Fig. 7 – Depth of 50 Per Cent Air Concentration as a Function of Discharge

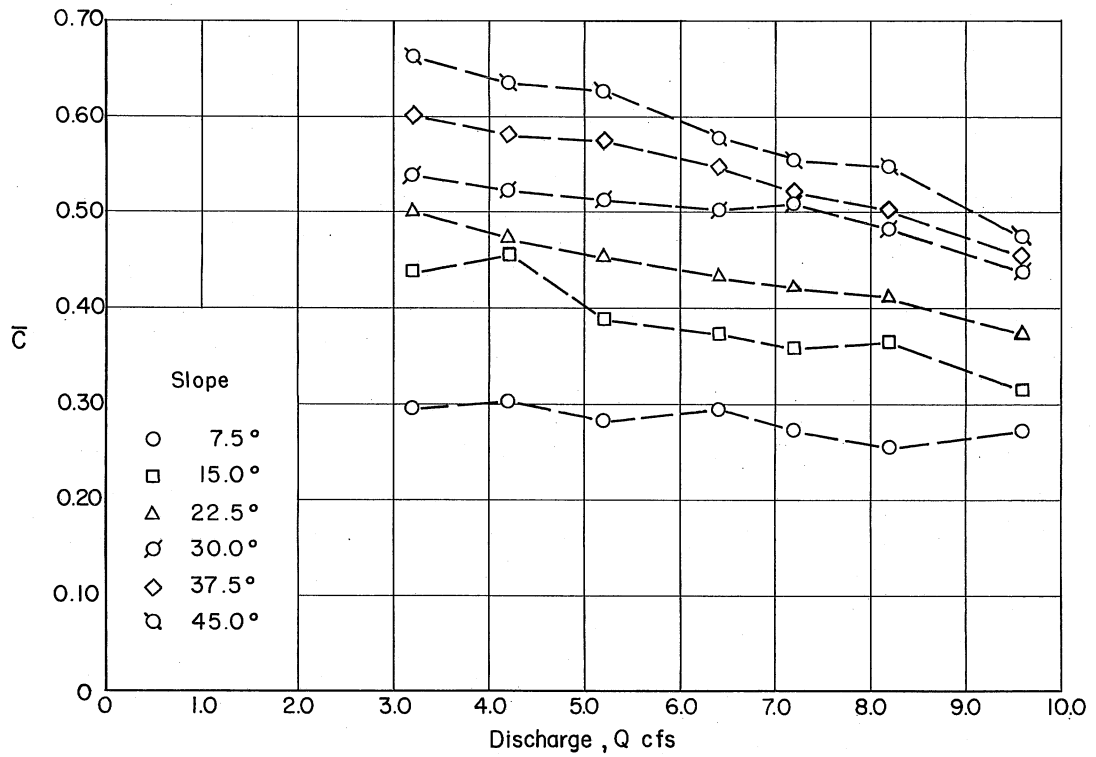

Fig. 8 – Mean Air Concentration of Total Flow as a Function of Discharge

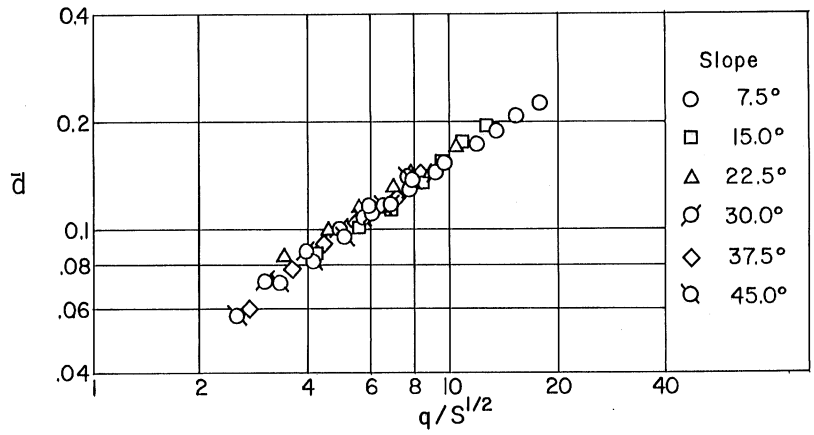

Fig. 9 – Mean Depth as a Function of $q/S^{1/2}$

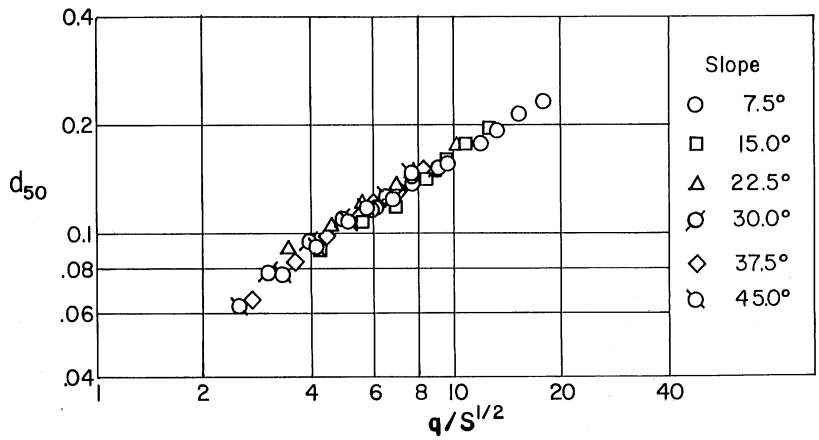

Fig. 10 – Depth of 50 Per Cent Air Concentration as a Function of $q/S^{1/2}$

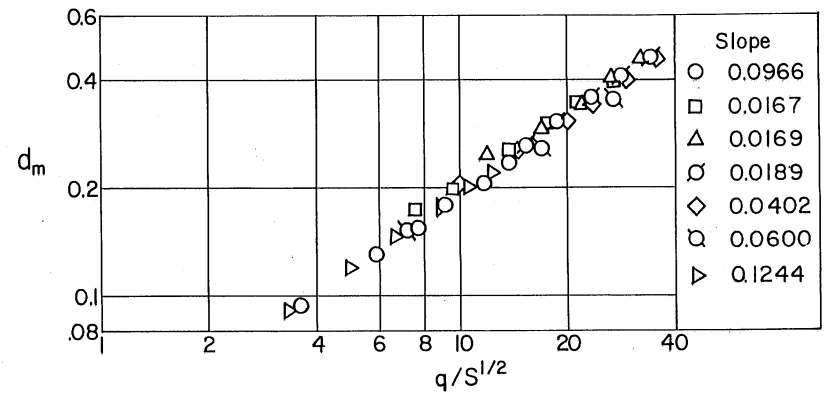

Fig. 11 – Depth of Unaerated Flow as a Function of $q/S^{1/2}$

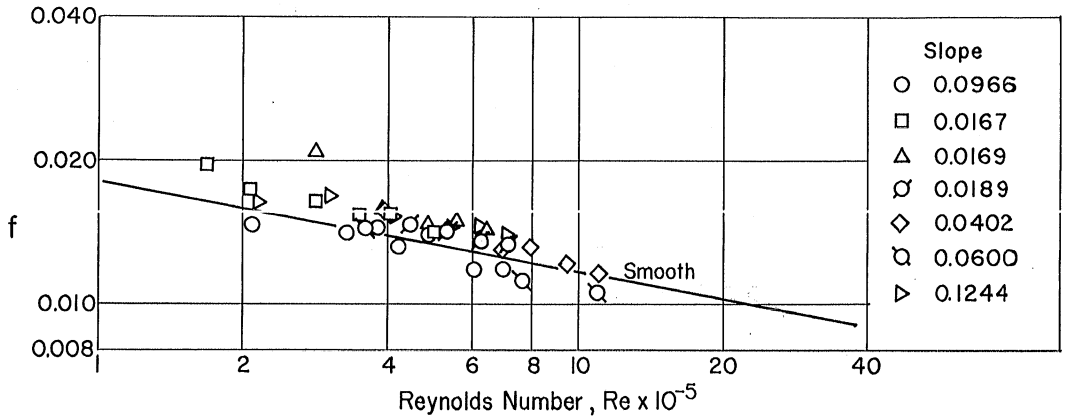

Fig. 12 – Friction Factor as a Function of Reynolds Number for Unaerated Flow

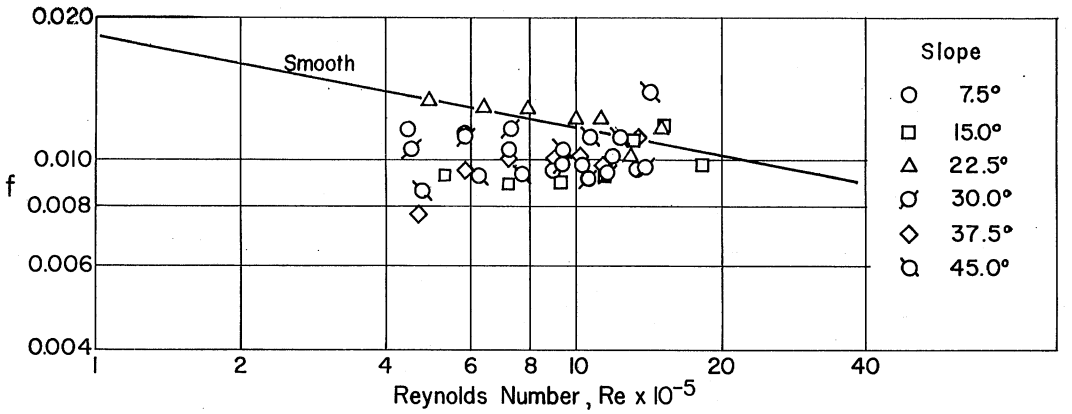

Fig. 13 – Friction Factor as a Function of Reynolds Number

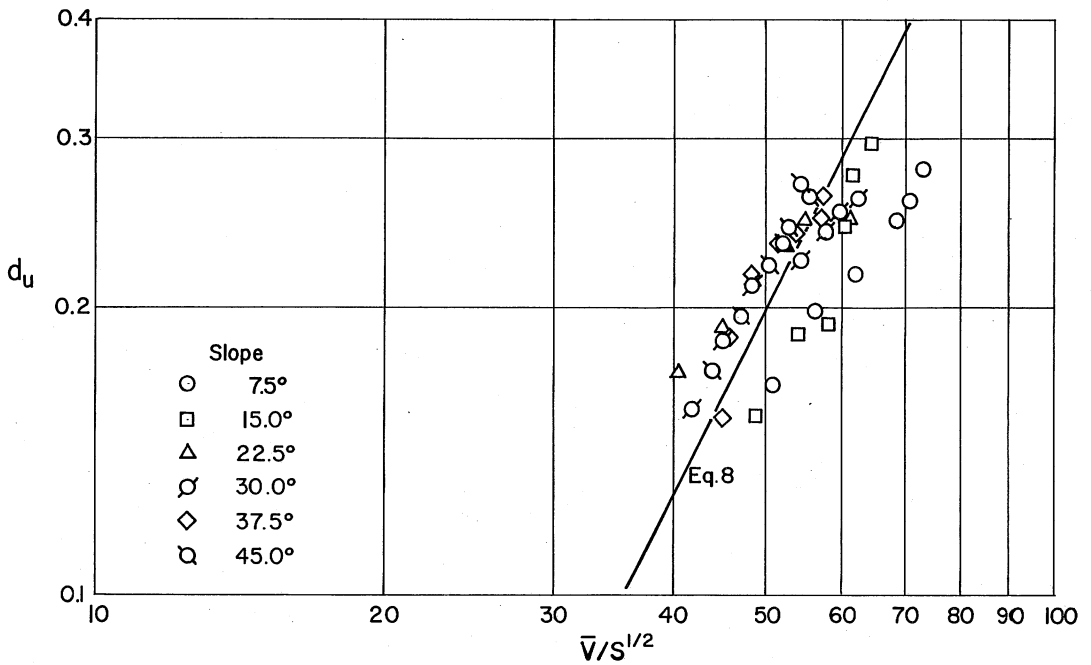

Fig. 14 – Maximum Depth as a Function of $V/S^{1/2}$

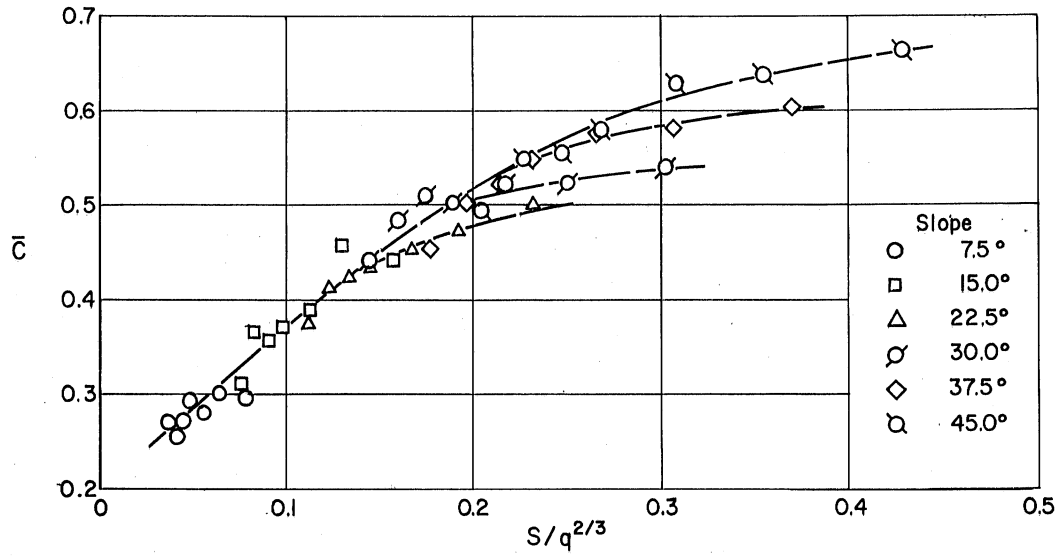

Fig. 15 - Mean Concentration of Total Flow as a Function of $S/q^{2/3}$

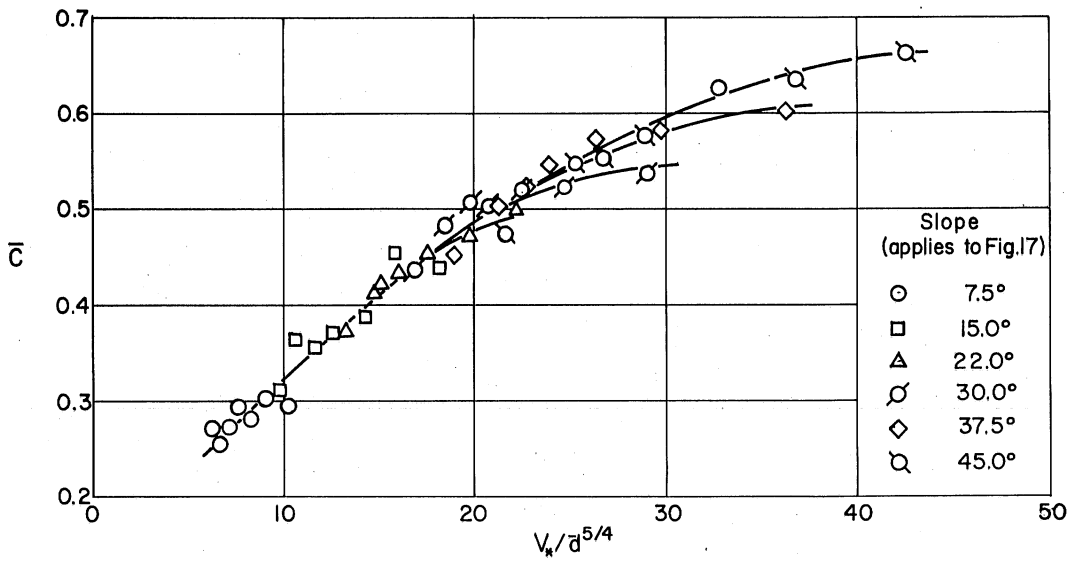

Fig. 16 - Mean Concentration of Total Flow as a Function of $V_*/(\bar{d})^{5/4}$

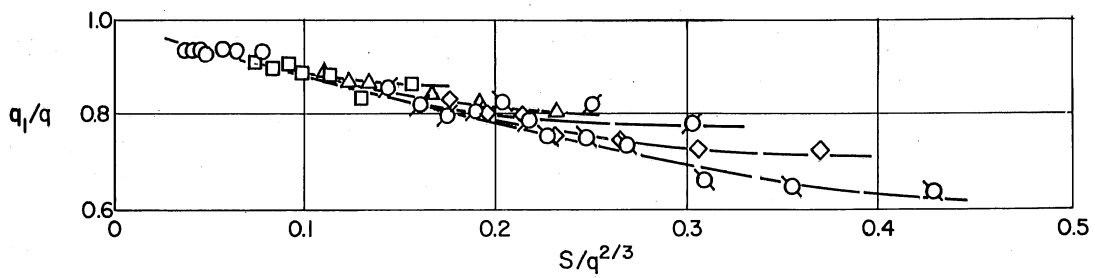

Fig. 17 - Relative Discharge Below Mean Depth as a Function of $S/q^{2/3}$

APPENDIX A

ANALYSIS OF AIR-CONCENTRATION DISTRIBUTION

APPENDIX A

ANALYSIS OF AIR-CONCENTRATION DISTRIBUTION

The general characteristics of the air-concentration distribution curves have been illustrated in the report (Fig. 4). From these observed data, it appears that the air-entrained flow is made up of two parts; a lower region where the air is transported as a suspension of air bubbles in the flowing water, and an upper region where water droplets or clumps of air and water are moving in the atmosphere above the main flow. Between the two regions is a transition depth where the character of the two regions changes. In the lower region the air distribution is governed by the turbulence fluctuations described by some boundary layer equation, while in the upper region each particle follows a trajectory, more or less independent of its neighbors, determined initially by the velocity fluctuations at the transition depth. The velocity fluctuations normal to the bed created by the turbulence of the flow in the lower portion are presumed to be great enough to penetrate the surface at the transition depth and to project the water particles into the atmosphere. The transition depth is necessarily a statistical mean of a fluctuating surface.

A. Air Distribution in Upper Region of Flow

If it is assumed that the normal components of the turbulent velocity fluctuations are randomly distributed about zero, those in the outward direction will constitute one-half of a Gaussian distribution. Since they are in or near the surface, the particles of water will be carried into the atmosphere against the force of gravity to an elevation proportional to the square of the individual velocities. Therefore, since the normal velocities of the particles are randomly distributed about zero, the heights of the trajectories that they will follow will also be randomly distributed about zero. (The path will be a long flat trajectory because of the longitudinal component of the local velocity.) Since the heights possess a Gaussian distribution, the frequency, $f(y')$, of particles projected a distance y' above the point of their origin may then be expressed as

$$f(y') = \frac{2}{h\sqrt{\pi}} e^{-\left(\frac{y'}{h}\right)^2} \qquad (A\text{-}1)$$

where h is a measure of the mean height, the particles are projected into the atmosphere. The factor 2 is used to indicate that only particles being projected outwardly are being considered. This indicated that $\int_0^\infty f(y')\,dy' = 1$ or that 1/2 a Gaussian distribution has been taken. Furthermore, since it is presumed that the flow is uniform on the average, particles are being projected at all points of the transitional surface so that only outward normal components need be considered.

The proportion of all particles leaving a unit area of the transition surface that reach or pass through a corresponding area at elevation y' will be

$$P_{y'} = \frac{2}{h\sqrt{\pi}} \int_{y'}^{\infty} e^{-\left(\frac{y'}{h}\right)^2} dy' \qquad (A\text{-}2)$$

and the number of particles reaching or passing through this area in both directions during the sampling period will be

$$N_{y'} = N_T P_{y'} \qquad (A\text{-}3)$$

where N_T is the total number of particles that leave or return to the transition surface during the sampling period. The average number of particles that reach or pass through any horizontal area per unit time may be assumed proportional to the average concentration of water particles. Therefore, the air concentration at any distance y' is determined from Eq. (A-3) and (A-2) in terms of the concentration of air at the transition level, C_T, and the representative height, h, as

$$1 - C = \frac{2(1 - C_T)}{h\sqrt{\pi}} \int_{y'}^{\infty} e^{-\left(\frac{y'}{h}\right)^2} dy' \qquad (A\text{-}4)$$

Equation (A-4) is, of course, the cumulative Gaussian probability curve and, in this case, is applicable for $y' > 0$. The concentration gradient, dc/dy, becomes

$$\frac{dc}{dy} = \frac{2(1 - C_T)}{h\sqrt{\pi}} \, e^{-\left(\frac{y'}{h}\right)^2} \tag{A-5}$$

when $y' = 0$, dc/dy is a maximum whose value is

$$\left(\frac{dc}{dy}\right)_{max} = \frac{2(1 - C_T)}{h\sqrt{\pi}} \tag{A-6}$$

and occurs where the air concentration is C_T. The parameter, h, could be computed from Eq. (A-6). The value of $(dc/dy)_{max}$ and C_T are properties of the air-concentration profiles (plotted in Figs. B-1 to B-7 in Appendix B). However, these are not suitable for the determination of C_T because within the experimental error the maximum gradient is essentially constant over a rather wide range of concentrations and hence, C_T is difficult to obtain. A small change in C_T results in a corresponding small change in h.

The test of Eq. (A-4) as a description of the air-concentration distribution in the upper regions of the flow then lies in the degree to which the measured air concentrations fit a cumulative Gaussian probability distribution. In all of the measured distribution curves, the depth, $d_{0.50}$, where the air concentration is 0.5, corresponds approximately to the region where the gradient is a maximum and to this extent may be used as the transition depth since Eq. (A-4) is relatively insensitive to a small change in C_T. Since Eq. (A-4) represents a straight line on arithmetic-probability paper, a plot of a typical experiment should plot as a straight line on such a graph if an equation such as Eq. (A-4) will represent the data. Figure A-1 is such a plot and shows that the air concentration in the upper region is distributed in accordance with the cumulative Gaussian curve. An increase or decrease in C_T of as much as 0.1 will shift the curve somewhat without changing its character. Similar results were obtained in all of the experiments. Equation (A-4), using $C_T = 0.5$, has been fitted to the measured concentration data

for the upper region of the flows and plotted with the experimental points in Figs. B-1 to B-7 in Appendix B. The choice of $d_{0.50}$ ($C_T = 0.5$) as the transition depth is quite arbitrary and is used only to test the form of the distribution. The true transition depth is governed by the boundary layer equation of the flow. The mean height of the water particles above the transition depth (here taken as d_{50}) has been measured from probability plots of the air concentration as indicated by Eq. (A-4) and plotted in Fig. A-2, as the ratio h/d_{50} as a function of $S/q^{2/3}$. It is interesting to note that a family of curves of the same type as those for other parameters results.

B. Air Distribution in the Lower Region of Flow

Using the same hypothesis of turbulent mixing, which served as the basis for the concentration distribution in the upper regions of the flow above the transition depth, the distribution of air in the lower portions below the transition depth will depend upon the turbulent mixing that occurs at all levels. The entrained air will be transported by the velocity fluctuations and distributed throughout the lower portions resulting in statistical equilibrium between the buoyancy of the air and the concentration gradient. The differential equation describing this equilibrium can be written as

$$C V_b = \epsilon_b \frac{dc}{dy} \qquad (A-7)$$

where C is again the air concentration at a normal distance, y, from the bed, V_b is the rising velocity of the air bubbles, and ϵ_b is a mixing parameter for the air bubbles transfer. The solution of Eq. (A-7) provides the air concentration as a function of depth. In aerated flows the value of ϵ_b as a function of y is unknown, and a number of assumptions as to the form of the function may be made. However, since it is presumed that the air bubbles are transported vertically in the same manner as the momentum transport in turbulent flow, it appears reasonable as an approximation to assume ϵ_b to be proportional to ϵ_m, the mixing parameter for turbulent flow. If it is assumed further that the distribution of the shear is the same in an aerated flow as in an unaerated flow, ϵ_b may be evaluated from

$$\tau = \tau_o \left(\frac{d_T - y}{d_T} \right) = \beta \rho \epsilon_b \frac{dv}{dy} \qquad (A\text{-}8)$$

where y is the normal distance from the bed where the velocity is V and the shear is τ. The boundary shear is τ_o, d_T is the transition depth that represents the upper limit of the turbulent mixing, ρ is the density of the mixture and β is the proportionality factor for $\epsilon_m = \beta \epsilon_b$. In the region near the bed where the velocity profile is assumed to be a logarithmic distribution [5], the velocity gradient may be evaluated as

$$\frac{dv}{dy} = \frac{\sqrt{\tau_o/\rho}}{ky} \qquad (A\text{-}9)$$

where in addition to the terms already defined, k is the Kármán universal constant. Substituting for ϵ_b in Eq. (A-7) the results of Eqs. (A-8) and (A-9), the differential equation for the air distribution becomes

$$C V_b = \frac{k\sqrt{\tau_o/\rho}}{\beta} \frac{(d_T - y)}{d_T} y \frac{dc}{dy} \qquad (A\text{-}10)$$

Integrating Eq. (A-10), assuming the air bubble velocity is independent of y, the air concentration as a function of y can be written as

$$C = C_o \left(\frac{y}{d_T - y} \right)^z \qquad (A\text{-}11)$$

in which

$$z = \frac{\beta V_b}{k\sqrt{\tau_o/\rho}} = \frac{\beta V_b}{kV_*} \qquad (A\text{-}12)$$

and C_o is the concentration at $y = d_T/2$. Plotted logarithmically (C vs $y/d_T - y$) Eq. (A-12) represents a straight line whose slope is numerically equal to z.

The use of Eq. (A-11) requires a knowledge of d_T, the transition depth, and should be applicable only in the region where the velocity profile is essentially logarithmic. Furthermore, it is not applicable in the region $y \longrightarrow d_T$ since the computed concentration becomes infinite. A plot of the measured concentrations in terms of the parameter, $y/d_T - y$, should result in a straight line when plotted logarithmically with the slope of the line and the constant C_o being governed by the choice of d_T. It is further required that z be a constant for each profile, that is, V_b is a constant. A plot of the measured air concentration in the lower region of the flow against the parameter $y/d_T - y$ is given in Fig. A-3 in which d_T was again arbitrarily taken as $d_{0.50}$. Since z must be evaluated from the experimental data, its value depends upon the choice of d_T. However, Eq. (A-11) is relatively insensitive to the choice of d_T within limits so that z varies accordingly. It is apparent that Eq. (A-11) fits the measured data very well to a distance nearly equal to $d_T(d_{0.50})$ in spite of the reduction in velocity in the neighborhood of the transition and departure from the logarithmic profile. See Figs. B-1 to B-7 in Appendix B.

The values of C_o and z have been determined from the experimental data from logarithmic plots of C against $y/d_T - y$ and are plotted in terms of $S/q^{2/3}$ in Figs. A-4 and A-5. The plot of C_o is similar to that for $\bar{C}$, showing an increase with $S/q^{2/3}$, and the development of a similar family of curves each having a different asymptote. The exponent z, on the other hand, has the hyperbolic form that corresponds to Eq. (A-12), since $S/q^{2/3}$ is a function of $V_*/(\bar{d})^{5/4}$.

The experimental results agree well with Eqs. (A-4) and (A-11), in spite of the arbitrary choice of the transition depth. The relative insensitivity of Eqs. (A-4) and (A-11) to small variations in the transition depth are accounted for in the empirical determination of the constants. Consequently, these equations are not suitable for the determination of the transition depth. The equations do suggest the nature of the mixing phenomena as an explanation of air-entrained flows.

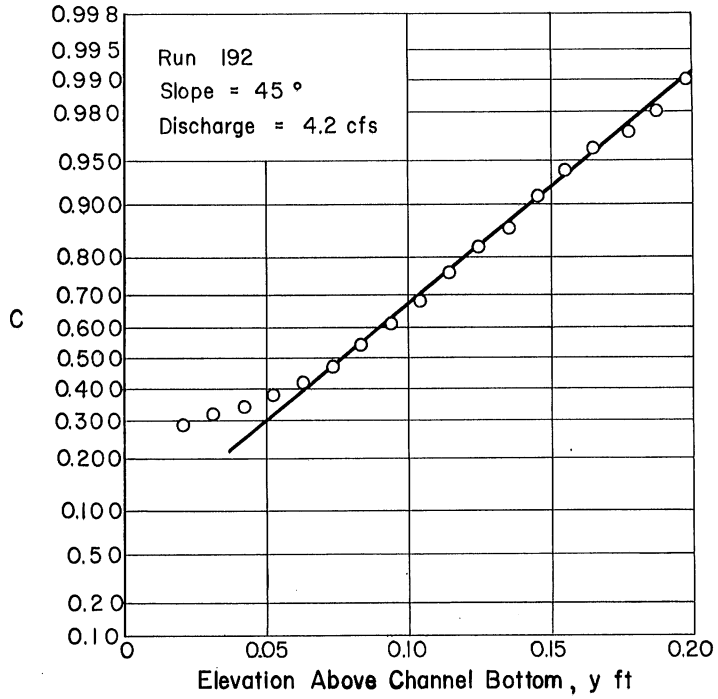

Fig. A-1 - Measured Air Concentration Plotted as a Probability Function

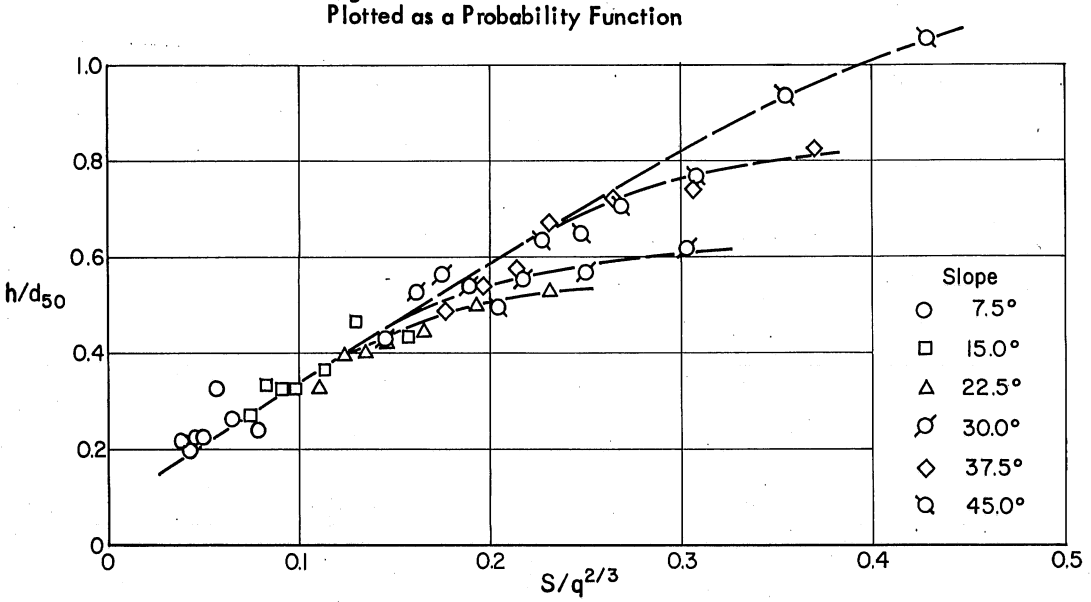

Fig. A-2 - Variation of h/d_{50} as a Function of $S/q^{2/3}$

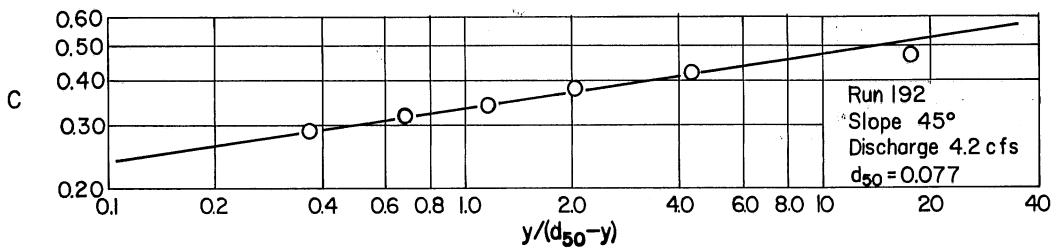

Fig. A-3 - Measured Air Concentration in Lower Region of Flow

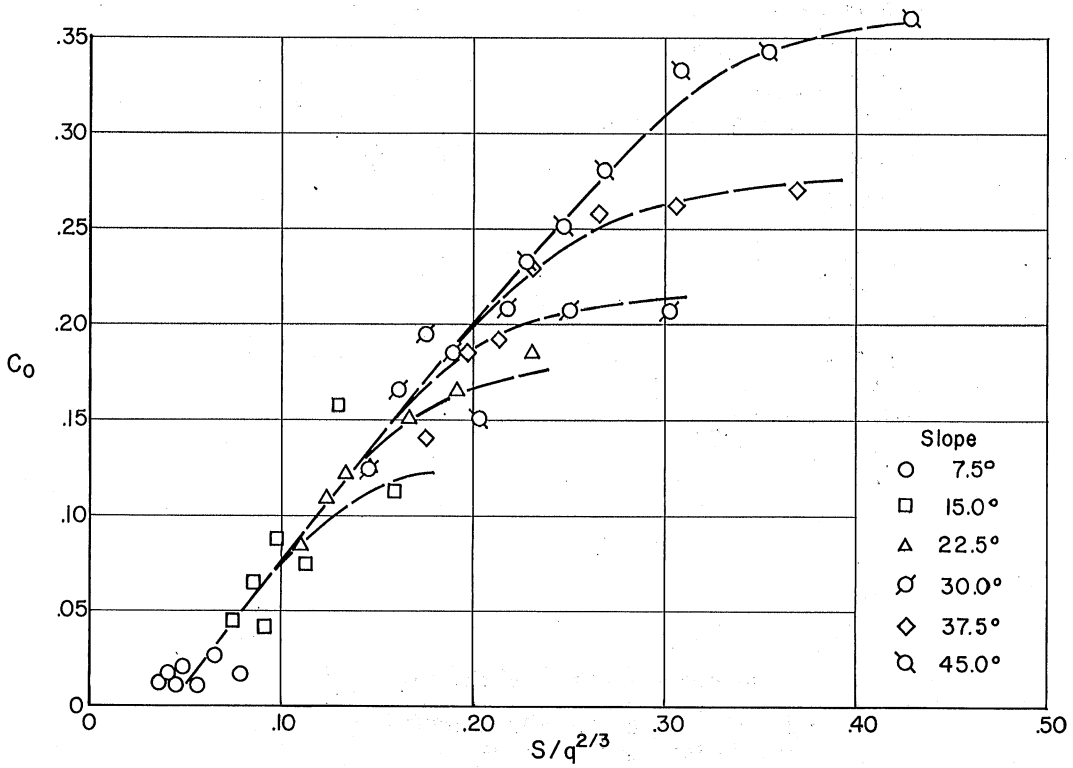

Fig. A-4 – Constant C_o (Eq. A-11) as a Function of Parameter $S/q^{2/3}$

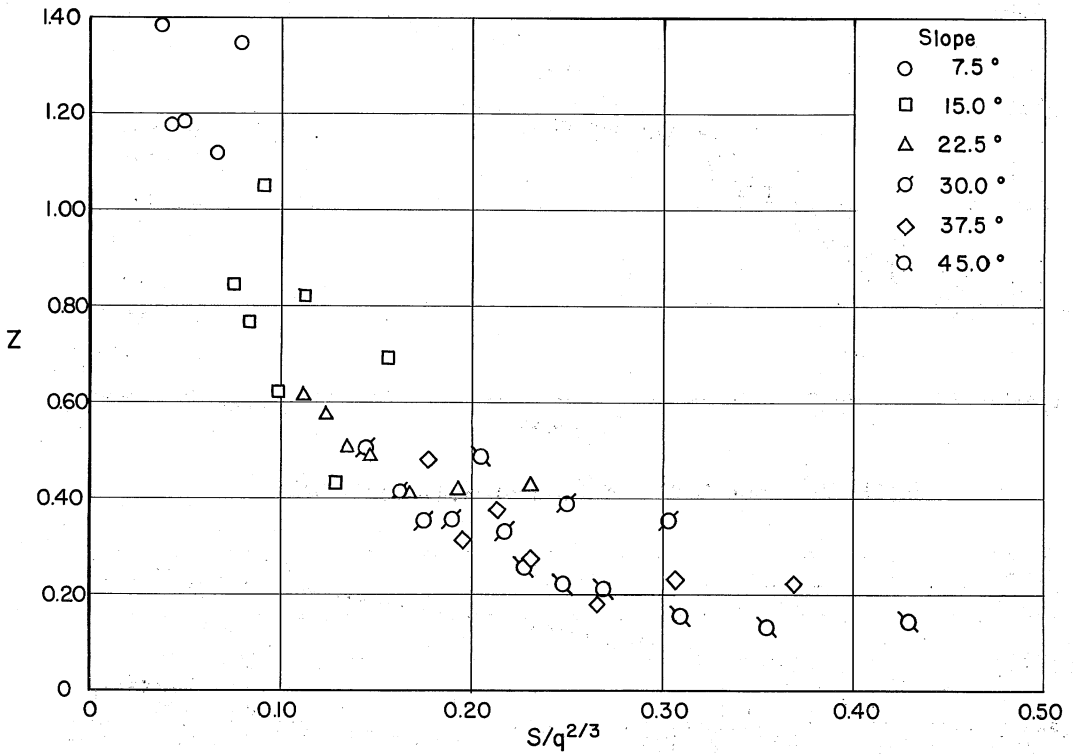

Fig. A-5 – Exponent z (Eq. A-11) as a Function of Parameter $S/q^{2/3}$

APPENDIX B

GRAPHICAL PRESENTATION OF EXPERIMENTAL MEASUREMENTS

A P P E N D I X B

GRAPHICAL PRESENTATION OF EXPERIMENTAL MEASUREMENTS

The experimental data have been plotted to show the air concentration at various normal distances from the bed. Superimposed upon each experimental set are curves representing Eq. (A-4) and Eq. (A-11) from Appendix A with the constants determined from the plots.

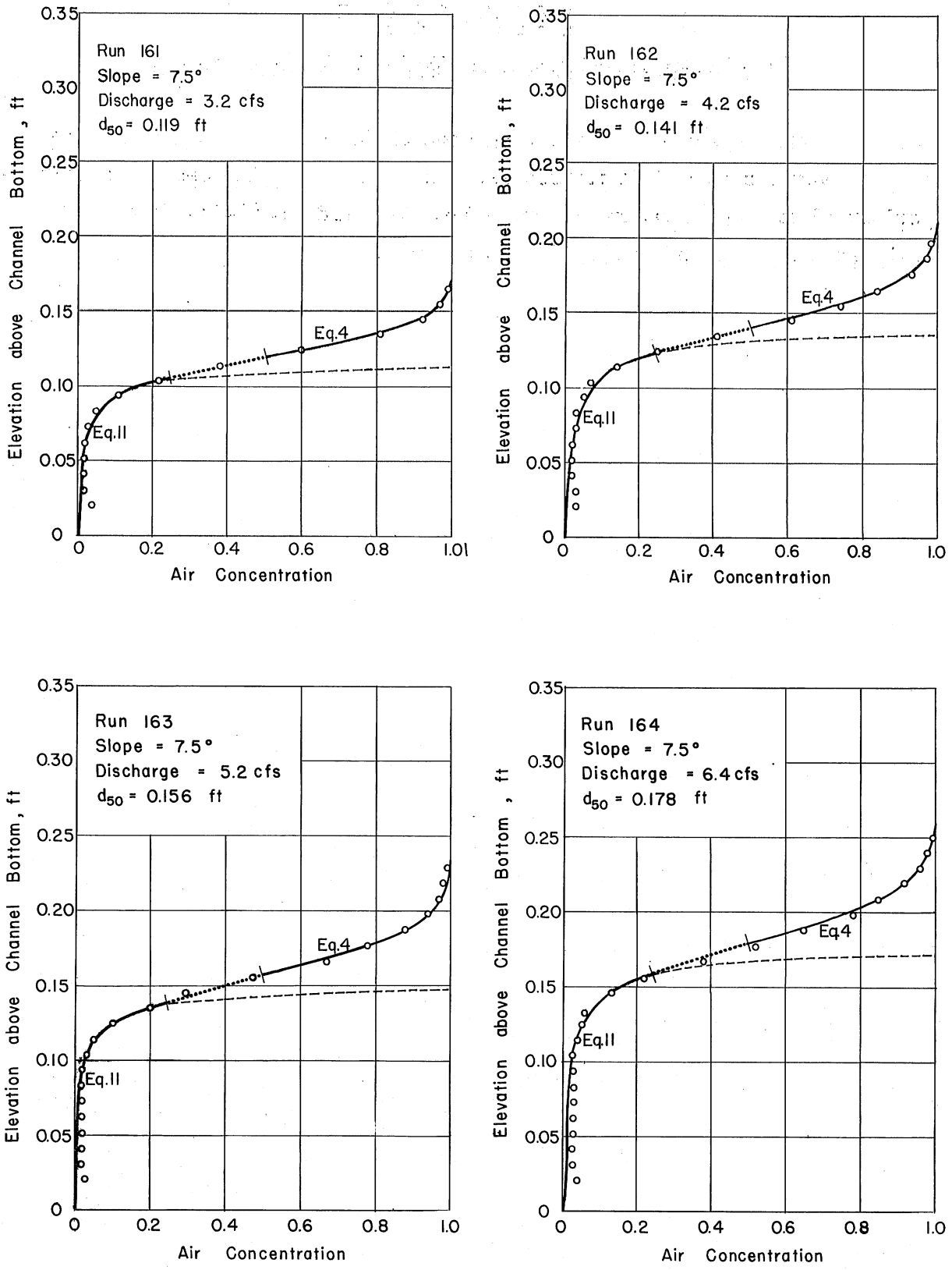

Fig. B-1 - Air-Concentration Distribution Slope 7.5°

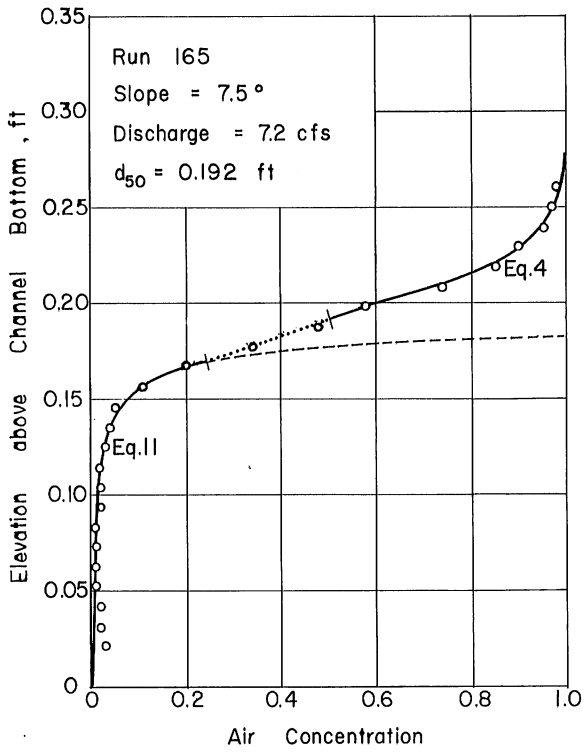

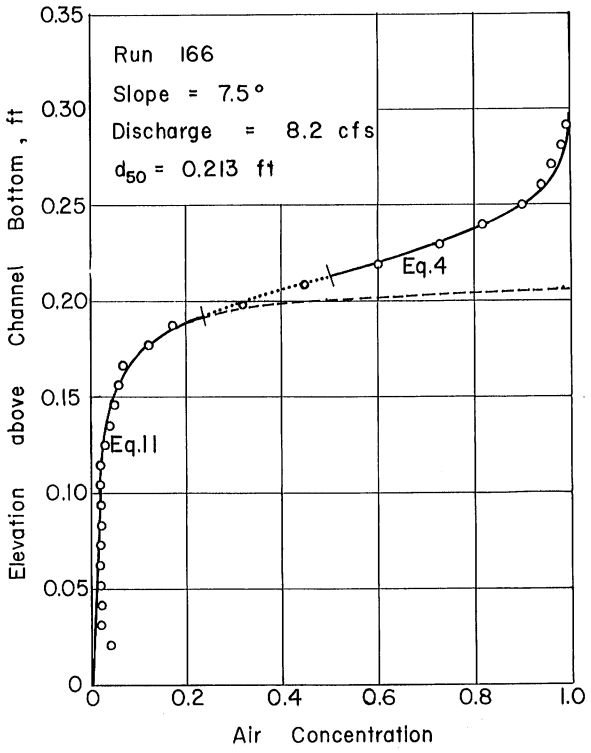

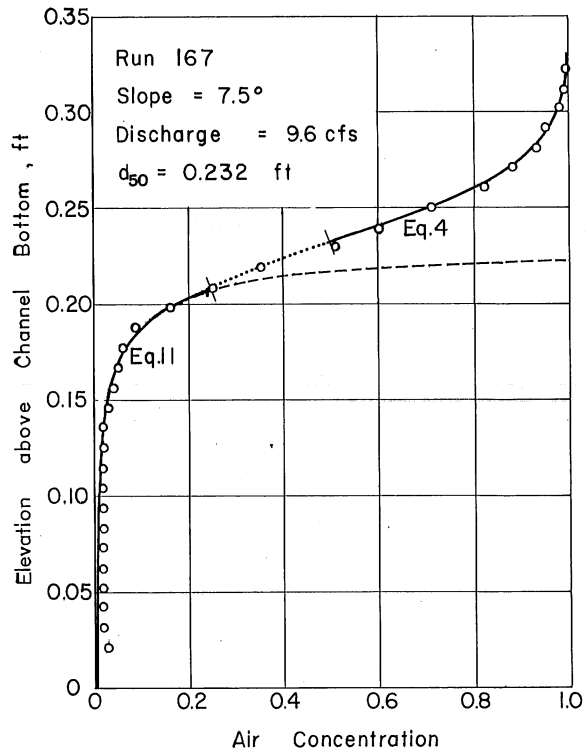

Fig. B-1 - Air-Concentration Distribution Slope 7.5°

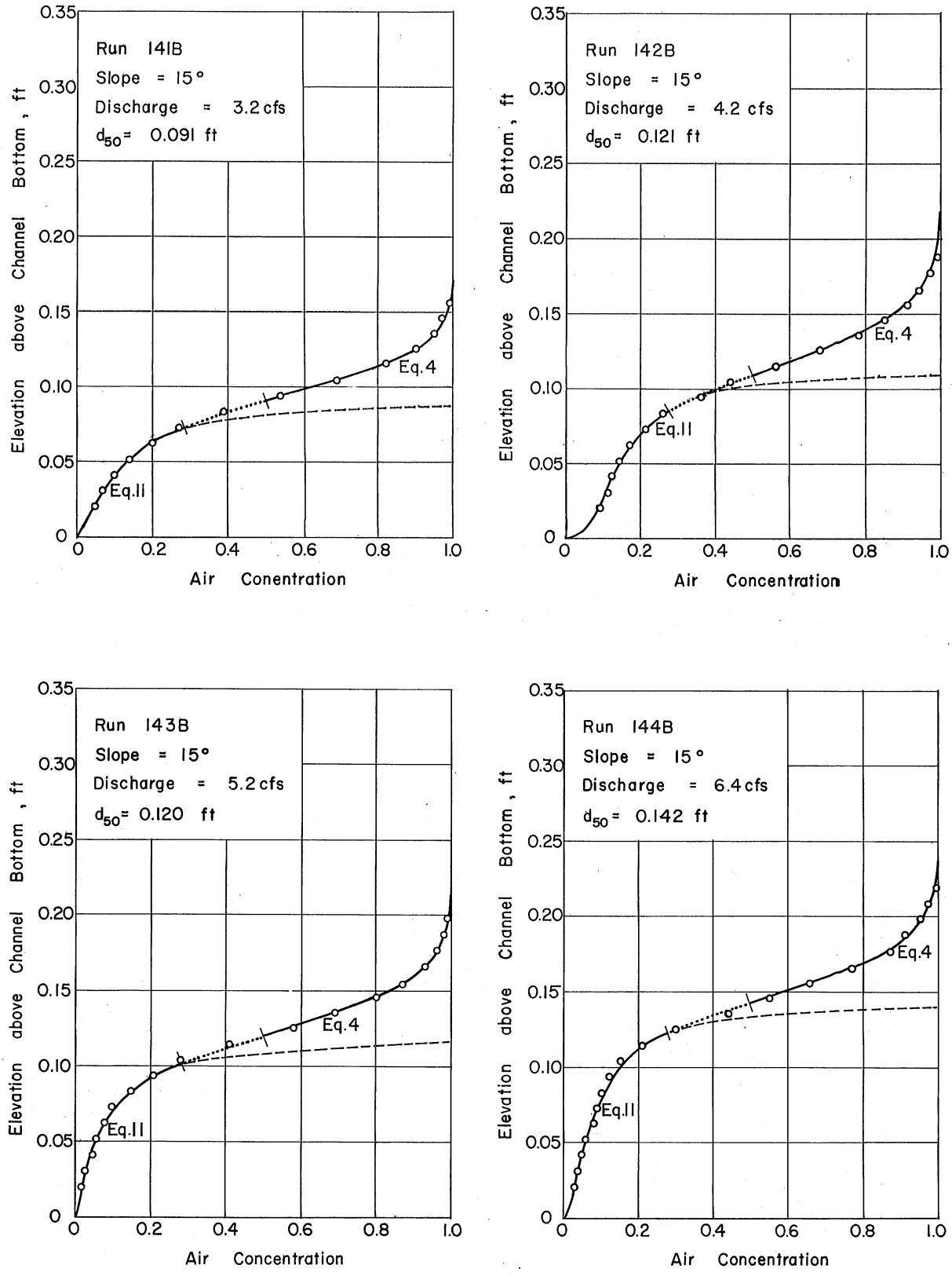

Fig. B-2 – Air-Concentration Distribution Slope 15°

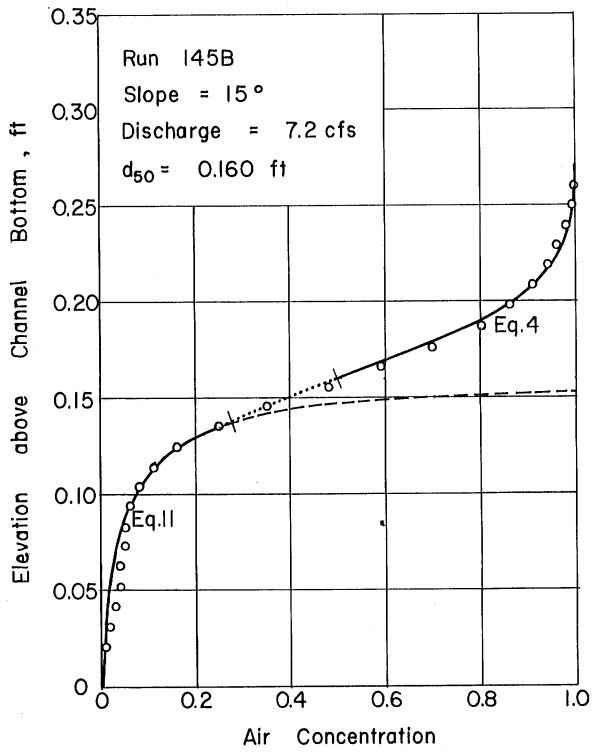

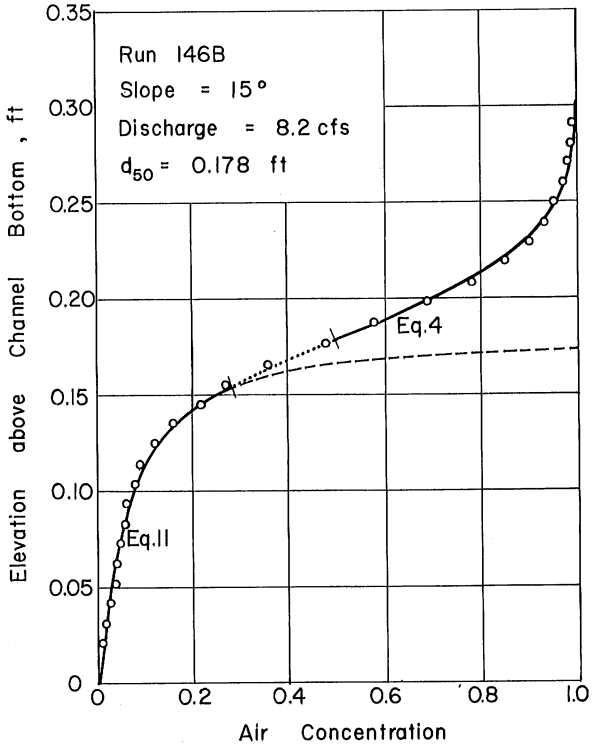

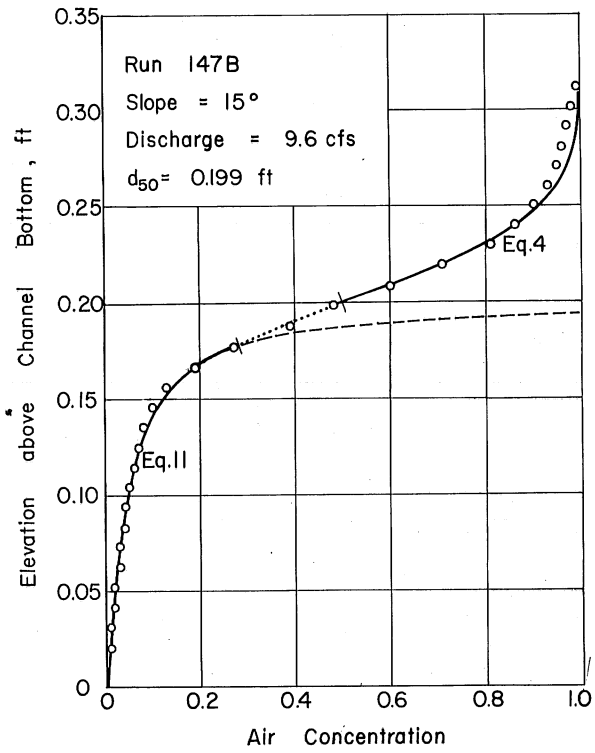

Fig. B-2 – Air-Concentration Distribution Slope 15°

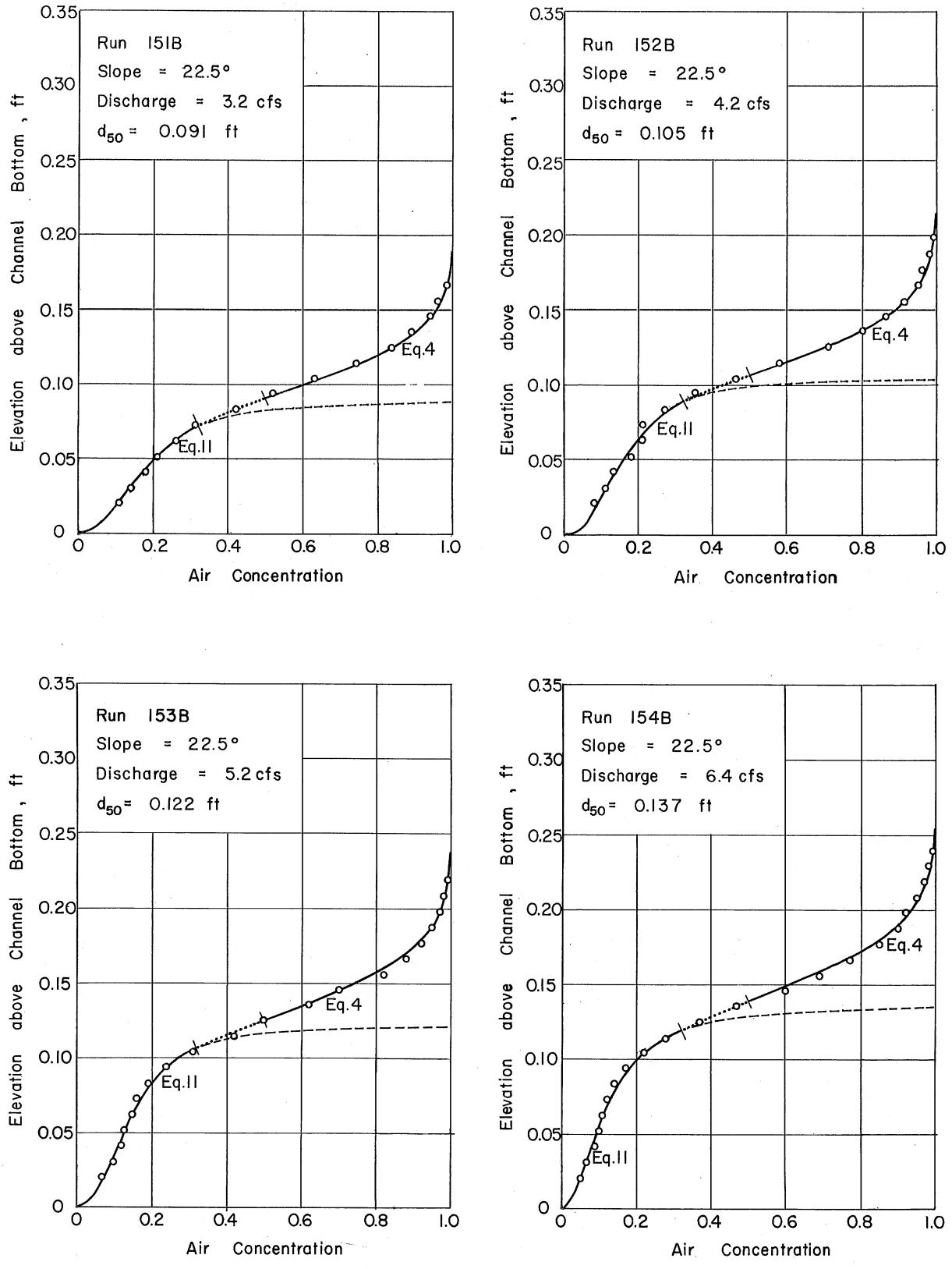

Fig. B-3 – Air-Concentration Distribution Slope 22.5°

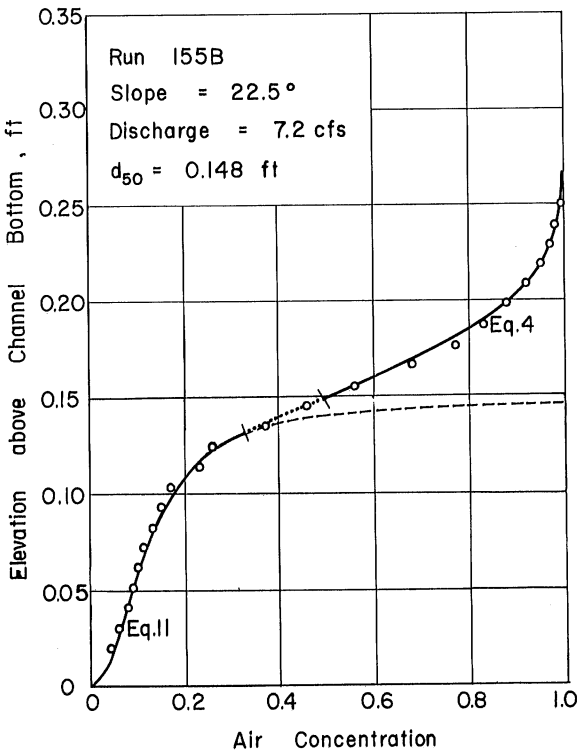

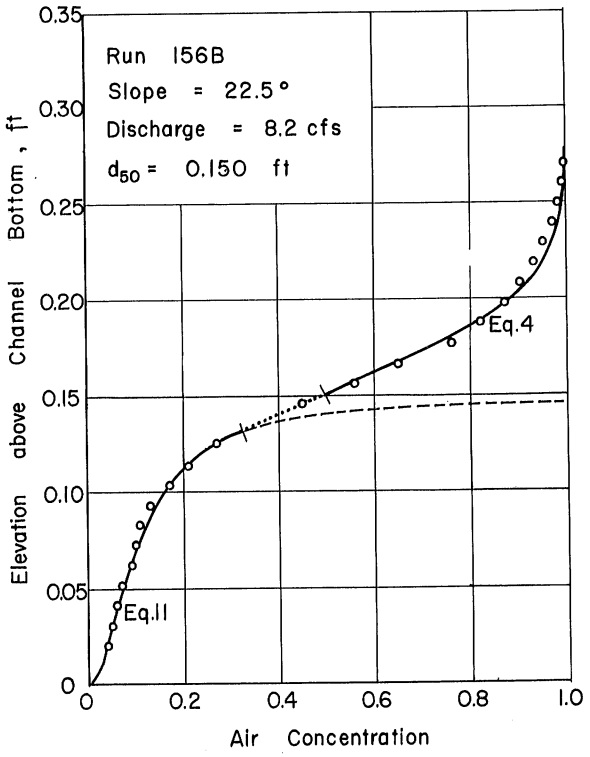

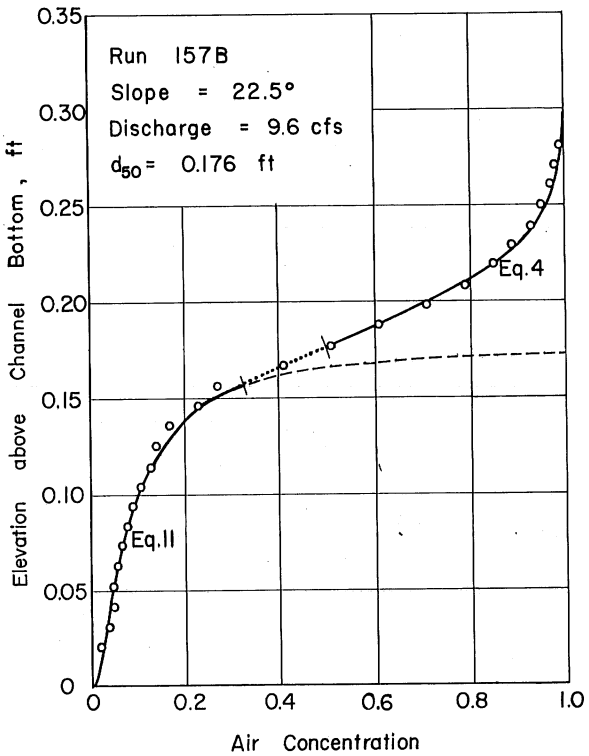

Fig. B-3 – Air-Concentration Distribution Slope 22.5°

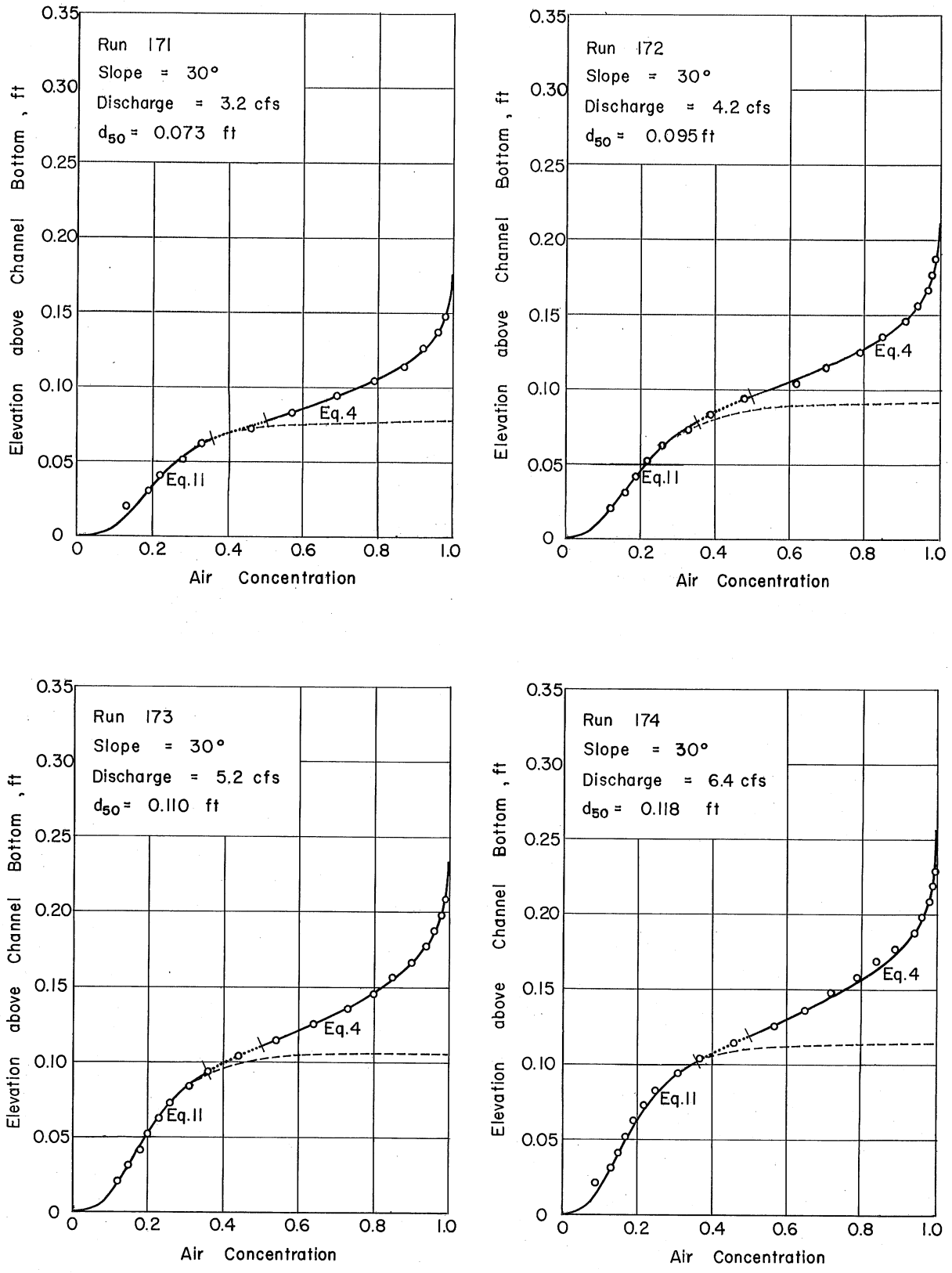

Fig. B-4 – Air-Concentration Distribution Slope 30°

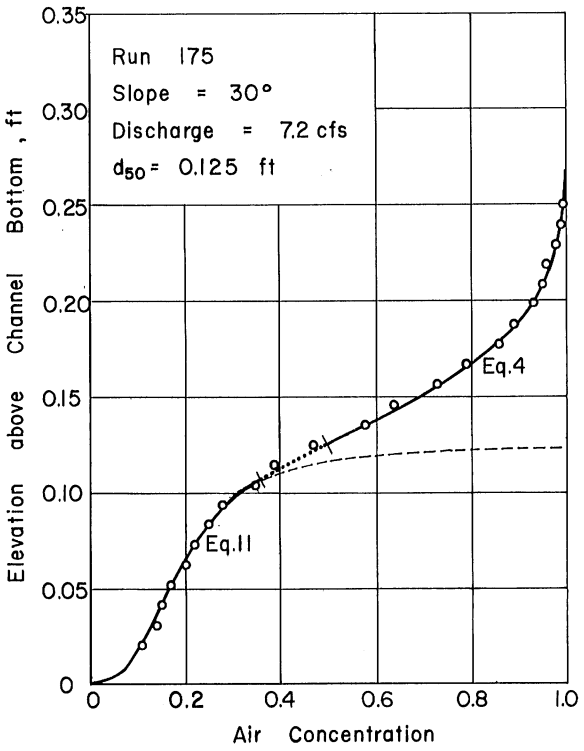

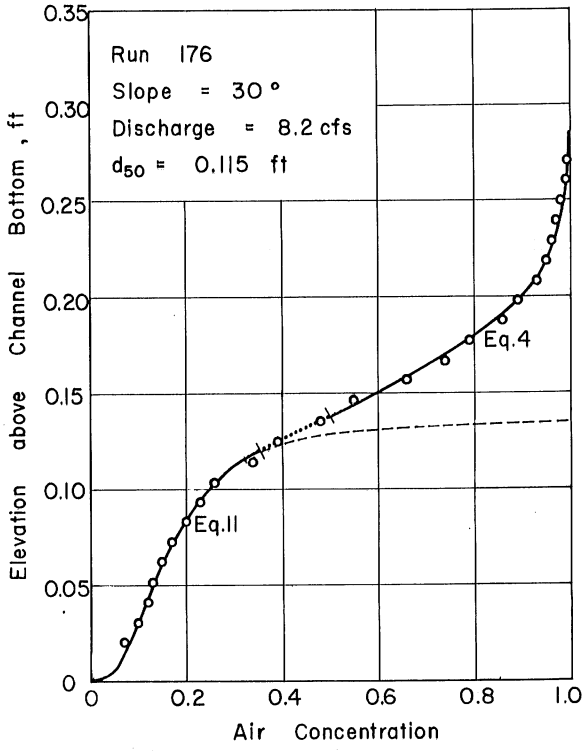

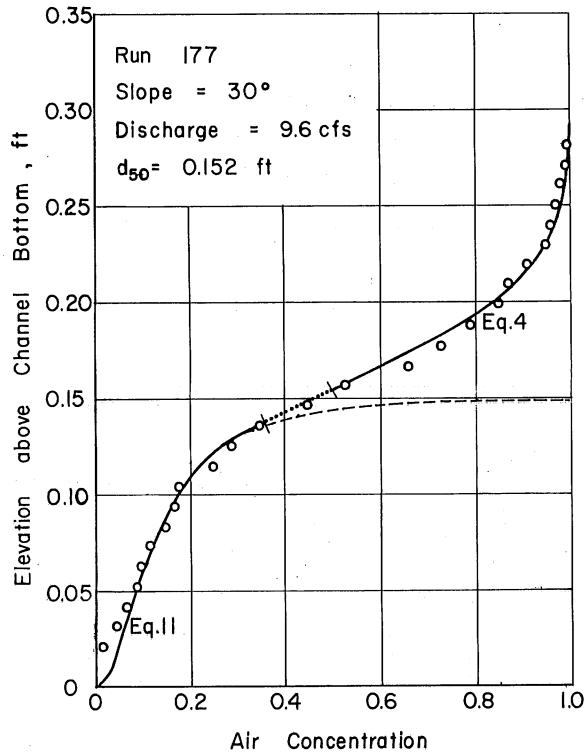

Fig. B-4 – Air-Concentration Distribution Slope 30°

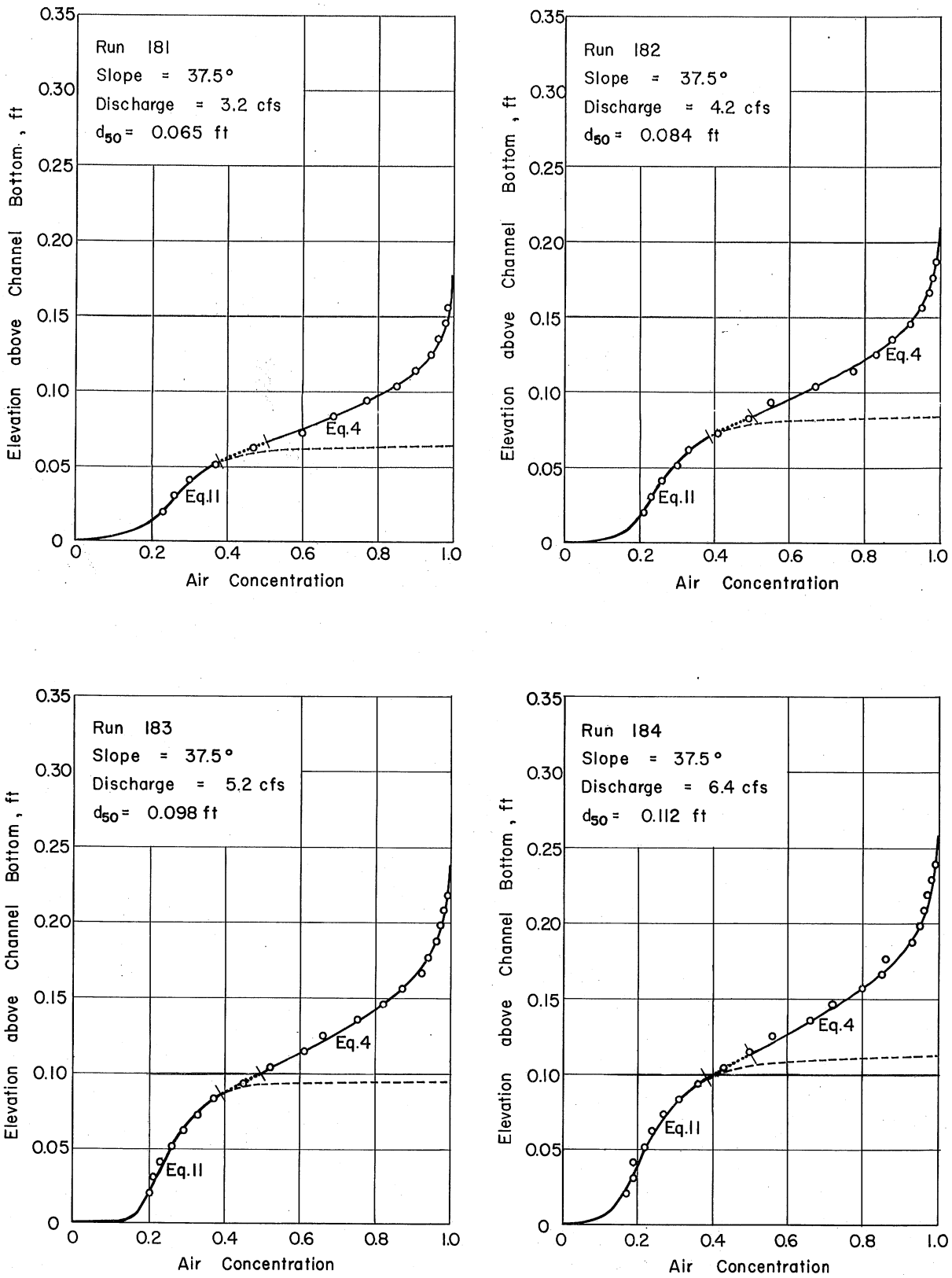

Fig. B-5 – Air-Concentration Distribution Slope 37.5°

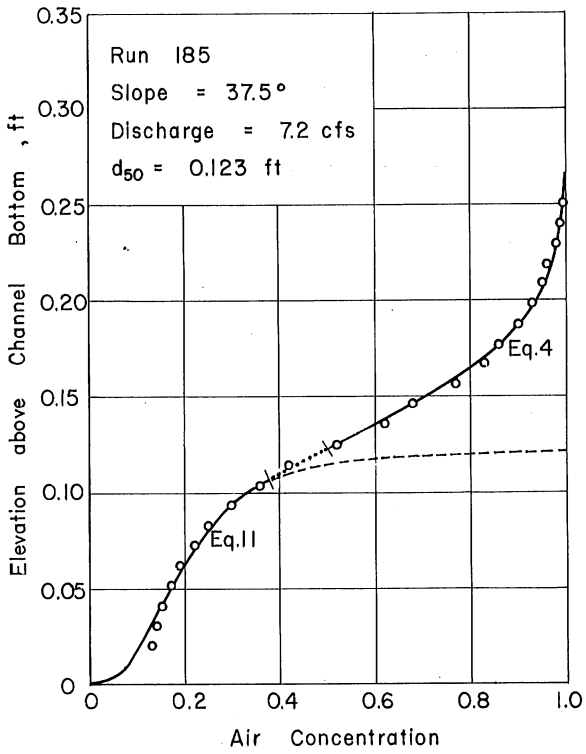

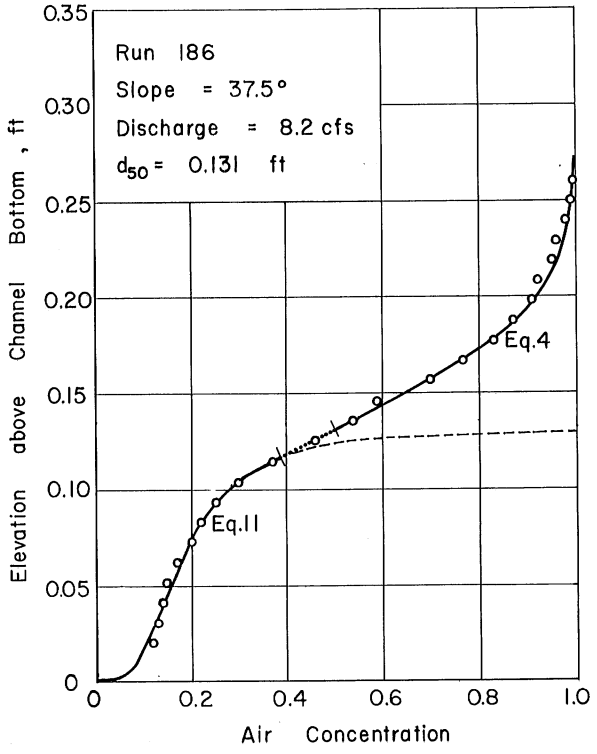

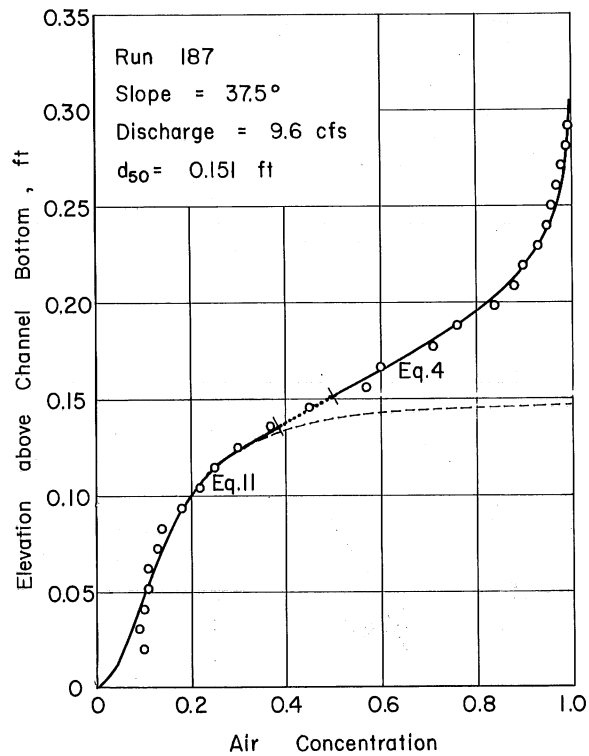

Fig. B-5 - Air-Concentration Distribution Slope 37.5°

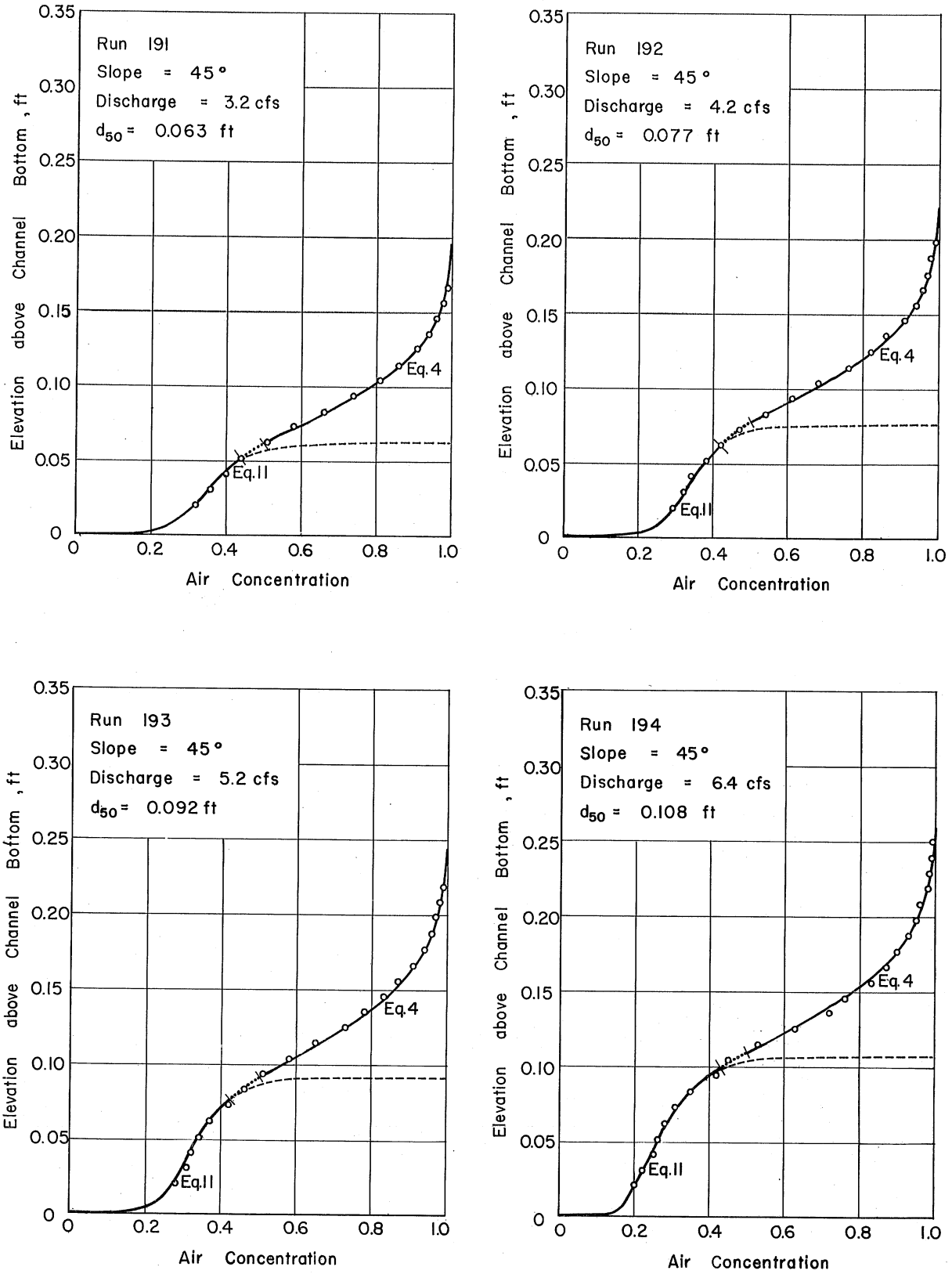

Fig. B-6 – Air-Concentration Distribution Slope 45°

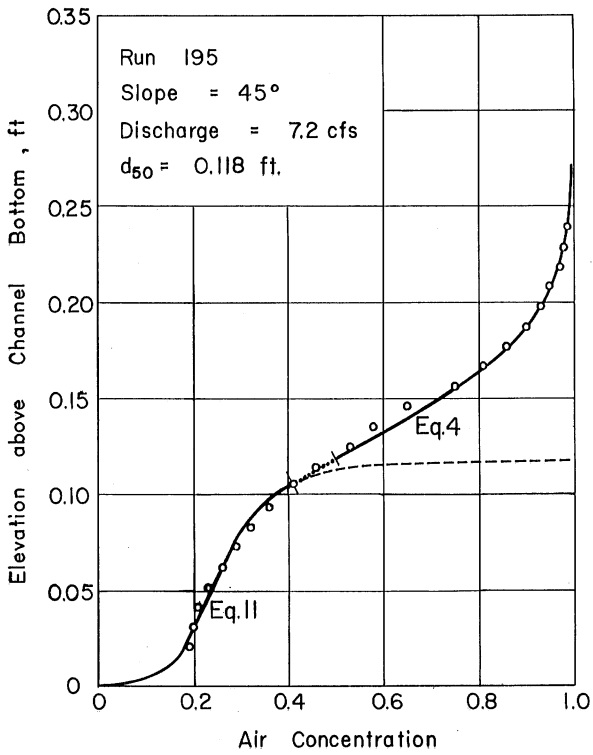

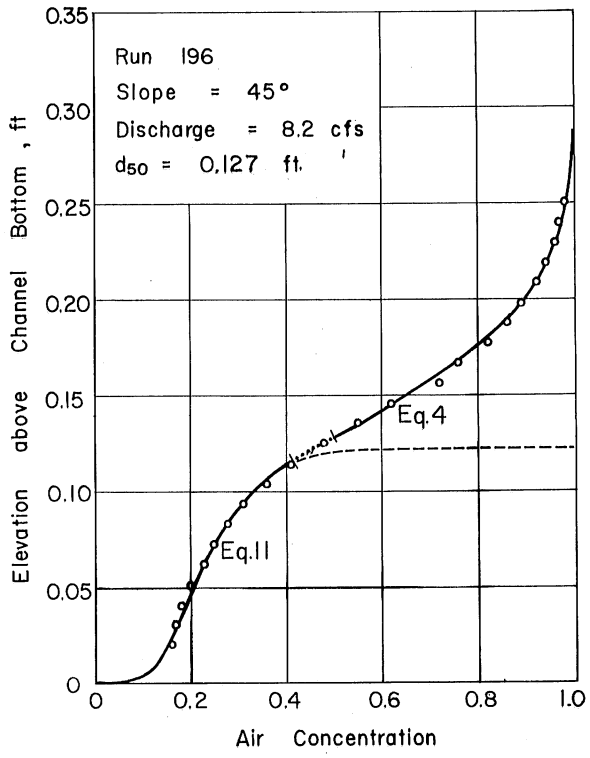

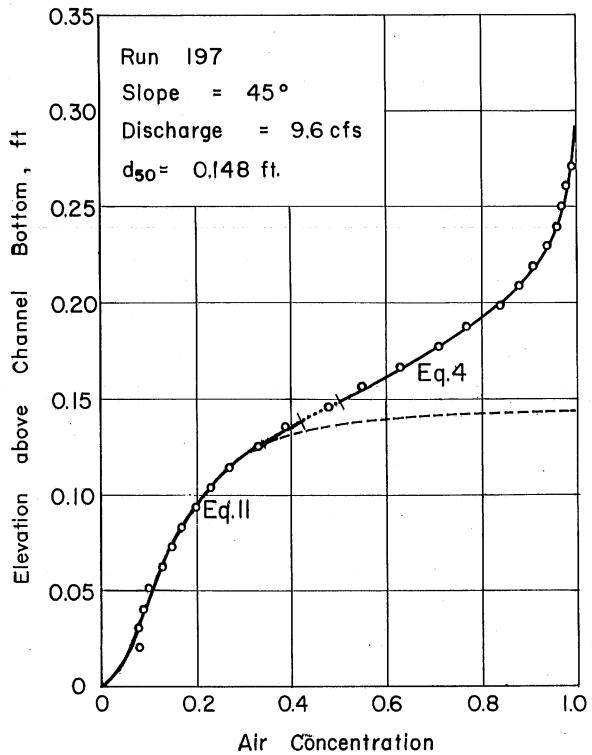

Fig. B-6 - Air-Concentration Distribution Slope 45°

DISTRIBUTION LIST FOR PROJECT REPORT NO. 48

of the St. Anthony Falls Hydraulic Laboratory

Copies	Organization
2	Chief of Naval Research, Navy Department, Washington 25, D. C., Attn: Code 438.
1	Commanding Officer, Office of Naval Research, Branch Office, The John Crerar Library Bldg., 86 East Randolph Street, Chicago 1, Illinois.
1	Commanding Officer, Office of Naval Research, Branch Office, 346 Broadway, New York 13, New York.
1	Commanding Officer, Office of Naval Research, Branch Office, 1030 East Green Street, Pasadena 1, California.
5	Commanding Officer, Office of Naval Research, Navy #100, Fleet Post Office, New York, New York.
6	Director, Naval Research Laboratory, Washington 25, D. C. Attn: Code 2021.
1	Chief, Bureau of Aeronautics, Navy Department, Washington 25, D. C., Attn: Research Division.
1	Chief, Bureau of Ordnance, Navy Department, Washington 25, D. C., Attn: Research and Development Division.
3	Chief, Bureau of Ships, Navy Department, Washington 25, D. C., Attn: [Research & Development (Code 300) (1), Preliminary Design & Ship Protection (Code 420) (1), Scientific, Structural & Hydrodynamics (Code 442) (1)].
1	Chief, Bureau of Yards and Docks, Navy Department, Washington 25, D. C., Attn: Research Division.
1	Commander, Naval Ordnance Test Station, 3202 E. Foothill Blvd., Pasadena, California, Attn: Head, Underwater Ord Dept.
3	Commanding Officer and Director, David Taylor Model Basin, Washington 7, D. C., Attn: [Hydromechanics Lab. (1), Seaworthiness & Fluid Dynamics Division (1), Library (1)].
1	Librarian, U. S. Naval Postgraduate School, Monterey, California.
1	Dr. J. H. McMillen, National Science Foundation, 1520 H Street, N.W., Washington, D. C.
2	Director, National Bureau of Standards, Washington 25, D. C. Attn: [Fluid Mechanics Section (1), Dr. G. H. Keulegan (National Hydraulic Lab.) (1)].

Copies	Organization
1	Director of Research, National Advisory Committee for Aeronautics, 1512 H Street, N.W., Washington 25, D. C.
1	Director, Langley Aeronautical Laboratory, National Advisory Committee for Aeronautics, Langley Field, Virginia.
1	Commander, Air Research and Development, Command, P. O. Box 1395, Baltimore 18, Maryland, Attn: Fluid Mechanics Division.
1	Director, Waterways Experiment Station, Box 631, Vicksburg, Mississippi.
1	Beach Erosion Board, U. S. Army Corps of Engineers, Washington 25, D. C.
1	Office of Ordnance Research, Department of the Army, Washington 25, D. C.
1	Office of the Chief of Engineers, Department of the Army, Gravelly Point, Washington 25, D. C.
1	Director, Ballistics Research Laboratory, Department of the Army, Aberdeen Proving Ground, Aberdeen, Maryland.
1	Commissioner, Bureau of Reclamation, Washington 25, D. C.
1	Director, Oak Ridge National Laboratory, P. O. Box P, Oak Ridge, Tennessee.
1	Director, Applied Physics Division, Sandia Laboratory, Albuquerque, New Mexico.
5	Armed Services Technical Information Agency, Documents Service Center, Knott Building, Dayton 2, Ohio.
1	Office of Technical Services, Department of Commerce, Washington, D. C.
1	Brown University, Division of Applied Mathematics, Providence, Rhode Island, Attn: Dr. George Morgan.
3	California Institute of Technology, Hydrodynamics Laboratory, Pasadena, California, Attn: Prof. F. C. Lindvall, Chairman, Steering Committee.
3	University of California, Berkeley 4, California, Attn: [Prof. H. A. Einstein, Dept. of Engineering (1), Prof. J. W. Johnson, Fluid Mechanics Lab. (1), Prof. H. A. Schade, Director, Engineering Research (1)].
1	Case Institute of Technology, Department of Mechanical Engineering, Cleveland, Ohio, Attn: Prof. G. Kuerti.

Copies	Organization
1	Cornell University, Graduate School of Aeronautical Engineering, Ithaca, New York, Attn: Prof. W. R. Sears, Director.
1	Harvard University, Department of Mathematics, Cambridge 38, Massachusetts, Attn: Prof. G. Birkhoff.
1	Indiana University, Department of Mathematics, Bloomington, Indiana, Attn: Prof. D. Gilbarg.
1	State University of Iowa, Iowa Institute of Hydraulic Research, Iowa City, Iowa, Attn: Dr. Hunter Rouse, Director.
1	Director, Applied Physics Laboratory, Johns Hopkins University, 8621 Georgia Avenue, Silver Spring, Maryland.
1	University of Maryland, Institute for Fluid Dynamics and Applied Mathematics, College Park, Maryland, Attn: Prof. M. H. Martin, Director.
2	Massachusetts Institute of Technology, Cambridge 39, Massachusetts, Attn: [Prof. A. T. Ippen, Hydrodynamics Lab. (1), Department of Naval Architecture (1)].
1	Michigan State College, Hydraulics Laboratory, East Lansing, Michigan, Attn: Prof. H. R. Henry.
1	University of Michigan, Applied Mechanics Department, Ann Arbor, Michigan, Attn: Prof. J. S. McNown.
1	University of Minnesota, St. Anthony Falls Hydraulic Laboratory, Minneapolis 14, Minnesota, Attn: Dr. L. G. Straub, Director.
1	New York University, Institute of Mathematical Sciences, 25 Waverly Place, New York 3, New York, Attn: Prof. R. Courant, Director.
1	University of Notre Dame, College of Engineering, Notre Dame, Indiana, Attn: Dean K. E. Schoenherr.
1	Pennsylvania State University, Ordnance Research Laboratory, University Park, Pennsylvania, Attn: Prof. G. F. Wislicenus.
1	Stanford University, Applied Mathematics and Statistics Laboratory, Stanford, California.
1	Stevens Institute of Technology, Experimental Towing Tank, 711 Hudson Street, Hoboken, New Jersey.
1	Mr. George Hickox, Program Director for Engineering Sciences, National Science Foundation, Washington 25, D. C.
1	Worcester Polytechnic Institute, Alden Hydraulic Laboratory, Worcester, Massachusetts, Attn: Prof. J. L. Hooper, Director.

Copies	Organization
1	Aerojet General Corporation, 6352 N. Irwindale Avenue, Azusa, California, Attn: Mr. C. A. Gongwer.
3	Serials Division, University of Minnesota Library, Minneapolis, Minnesota.